

Holographic Photosynthesis

Irina Aref'eva and Igor Volovich

*Steklov Mathematical Institute, Russian Academy of Sciences,
Gubkina str. 8, 119991, Moscow, Russia*

E-mail: arefeva@mi.ras.ru, volovich@mi.ras.ru

ABSTRACT: There are successful applications of the holographic AdS/CFT correspondence to high energy and condensed matter physics. We apply the holographic approach to photosynthesis that is an important example of nontrivial quantum phenomena relevant for life which is being studied in the emerging field of quantum biology. Light harvesting complexes of photosynthetic organisms are many-body quantum systems, in which quantum coherence has recently been experimentally shown to survive for relatively long time scales even at the physiological temperature despite the decohering effects of their environments.

We use the holographic approach to evaluate the time dependence of entanglement entropy and quantum mutual information in the Fenna-Matthews-Olson (FMO) protein-pigment complex in green sulfur bacteria during the transfer of an excitation from a chlorosome antenna to a reaction center. It is demonstrated that the time evolution of the mutual information simulating the Lindblad master equation in some cases can be obtained by means of a dual gravity describing black hole formation in the AdS-Vaidya spacetime. The wake up and scrambling times for various partitions of the FMO complex are discussed.

KEYWORDS: holography, AdS/CFT correspondence, photosynthesis, light-harvesting complex, black holes, entanglement entropy, mutual information

Contents

1	Introduction	2
2	Setup	4
2.1	FMO complex	4
2.1.1	Seven bacteriochlorophylls	4
2.1.2	Master equation	5
2.1.3	Entropy of entanglement and mutual information	6
2.1.4	Reductions of the FMO complex	6
2.2	Holographic entanglement entropy	7
2.2.1	Static AdS background	7
2.2.2	Time dependent AdS Vaidya background	9
2.3	Iterative procedure to calculate $\mathcal{S}(A_1 \cup A_2 \cup \dots \cup A_n)$	11
2.4	Holographic mutual information	16
3	Holographic studies of simplest FMO complex	17
3.1	Holographic entanglement entropy for two site system during a quench at nonzero temperature.	17
3.2	Holographic mutual information for two site system at nonzero temperature.	19
3.3	Matching holographic calculations to the simulation results.	21
3.4	Wake up and scrambling times	22
4	Holographic studies of the FMO complex with one composite part	24
4.1	Phase structure of holographic entanglement entropy $S(A \cup B \cup C)$ for the Vaidya shell in the AdS_d black brane background	24
4.2	Mutual information for $(1, 6 3)$ -reduction of the FMO complex and scrambling time	26
4.3	Matching holographic calculations to the simulation results.	30
5	Conclusions	31
6	Acknowledgments	32

1 Introduction

The anti-de Sitter - conformal field theory (AdS/CFT) correspondence [1] and more general holographic gravity/gauge duality play an important role in modern theoretical physics. They have been used for description of strong interacting equilibrium and non-equilibrium systems in high energy physics, in particular, to describe heavy-ion collisions and formation of quark-gluon plasma [2–4], as well as in condensed matter physics [5, 6].

According to the holographic correspondence the quantum gravity (string theory) on anti-de Sitter spacetime (AdS) is equivalent to a certain quantum field theory on the AdS boundary. The holographic approach provides a powerful method for studying strongly coupled quantum field theories by means of the dual classical gravitational theory in the AdS space which is more tractable.

In last years, there has been a growing interest to study the entanglement entropy and quantum mutual information for various quantum systems by using the holographic approach [7]-[31] and refs therein. The entanglement entropy of a boundary region is determined by the area of the minimal bulk surface that coincides with the entangling surface at the boundary [7–9].

In this paper we apply the holographic approach to photosynthesis. Light harvesting complexes (LHC) in bacteria and plants are important examples of nontrivial quantum phenomena relevant for life which are being studied in the emerging field of quantum biology. Recent investigations of quantum effects in biology include also the process of vision, the olfactory sense, the magnetic orientation of migrant birds as well as photon antibunching in proteins, the quantum delocalization of biodyes in matter-wave interferometry and quantum tunneling in biomolecules, see for instance [32–37].

Photosynthesis is vital for life on Earth [38]. Photosynthesis changes the energy from the sun into chemical energy and splits water to liberate oxygen and convert carbon dioxide into organic compounds, especially sugars. Nearly all life either depends on it directly as a source of energy, or indirectly as the ultimate source of the energy in their food.

Light-harvesting complexes in plants and photosynthetic bacteria include protein scaffolds into which pigment molecules are embedded, e.g. chlorophyll or bacteriochlorophyll molecules. The pigment molecules absorb light and the resulting electronic excitation, exciton, is transported between the pigment molecules until it reaches a reaction center complex, where its energy is converted into separated charges. The process whereby the light energy is transported through the cell is extremely efficient – higher than any artificial energy transport process.

One models many photosynthetic light harvesting complexes by a general three-part structure comprising the antenna, the transfer network, and the reaction center. The antenna captures photons from sunlight and subsequently excites the electrons of the pigment from their ground state. The excited electrons, which combine with holes to make excitons, travel from the antenna through an intermediate protein exciton transfer complex to the reaction center where they participate in the chemical reaction that generates oxygen.

Quantum coherences have been observed in two-dimensional spectroscopic studies of energy transfer within several different light harvesting complexes. The simplest light

harvesting complex is the Fenna-Matthews-Olson (FMO) protein-pigment complex in green sulfur bacteria. We demonstrate that some numerical results on the time evolution of the mutual information for the FMO complex [39] can be obtained by using the holographic approach.

Experiments with the FMO complex have shown the presence of quantum beats between excitonic levels at both cryogenic ($77^\circ K$) and ambient ($300^\circ K$) temperatures [40–43]. Quantum coherence has also been seen in light harvesting antenna complexes of green plants [44] and marine algae [45]. There are also studies of quantum coherence within the reaction center [46].

Theoretical studies of excitation dynamics in the FMO complex in the single excitation subspace have demonstrated the presence of long-lived, multipartite entanglement. A study of the temporal duration of entanglement in the FMO complex using a simulation of excitation energy transfer dynamics under conditions that approximate the real environment was performed in [47]–[52]. Entanglement within the Markovian description of the FMO complex has been considered in [48, 51]. The time evolution of the mutual information in the FMO complex was studied in [50] by using simulation of the Gorini-Kossakowski-Sudarshan-Lindblad master equation. Quantum nonlocality as a function of time is studied in [53].

The paper is organized as follows.

In Sect.2 has an introductory character. Here we remind the main objects and tools of our study of the FMO complex. In Sect.2.1 has an introductory character. Here we briefly describe the FMO complex and write down the corresponding master equation. In Sect.2.1.3 the standard consideration of LHC as quantum system and entropy of entanglement and mutual information for the FMO complex are sketched. In Sect.2.1.4 we list different reductions of the FMO complex used in modern theoretical studies. In Sect.2.2 definitions of holographic entanglement entropy and mutual information, as well as the basic formula that we use in the main text are presented. In Sect.2.3 two iterative procedures to calculate the holographic entanglement entropy $\mathcal{S}(A_1 \cup A_2 \cup \dots \cup A_n)$ are presented. The first one takes into account contributions only of primitive diagrams and the second one incorporates also Boltzmann rainbow diagrams. In Sect.2.4 we remind the phase structure of the holographic mutual information $I(A, B)$ for two belts in the static backgrounds, empty AdS_{d+1} and AdS_{d+1} black brane.

Sect.3 is devoted to the study of the time evolution of holographic mutual information for the simplest reduction of the FMO complex. We start, Sect.3.1, by calculation of holographic entanglement entropy for two site system during a quench at nonzero temperature. Then in Sect.3.2 we study holographic mutual information for two site system at nonzero temperature. In Sect.3.3 we compare the results of our calculations with the mutual information $I(A, B)$ calculated for the reduced FMO system in [50]. In Sect.3.4 we discuss the dependencies of wake up time and scrambling times on the geometrical parameters and the initial temperature.

In Sect.4 we consider the holographic mutual information for the reduction of the FMO complex with one composite part. For this purpose in Sect.4.1 we study the phase structure of holographic entanglement entropy $S(A \cup B \cup C)$ for the Vaidya shell in the AdS_d black

brane background. In Sect.4.2 the mutual information for 3 segments and scrambling time for this background is calculated and in Sect.4.3 we make a fit of time dependence of the mutual information at the physiological temperature ($300^\circ K$) calculated in [50] for one mixed state by the time dependence of the holographic mutual information $I(A_1 \cup A_6, A_3)$ under the global quench by the Vaidya shell in AdS_4 .

2 Setup

2.1 FMO complex

2.1.1 Seven bacteriochlorophylls

The FMO protein complex [39] is the main light-harvesting component of the green sulfur bacteria *Prosthecochloris aestuarii*. It is a trimer, consisting of three identical molecular sub-units, Fig.1A. Each of the sub-units is a network of seven¹ interconnected bacteriochlorophylls $\{1, 2, \dots, 7\}$ arranged in two weakly connected branches that are separately connected to the antenna (bacteriochlorophyll sites one and six) and jointly connected to the reaction center via site three, Fig.1B.

The theoretical models in the literature [48–51] study the dynamics of one sub-unit of the trimer. The total Hamiltonian of the system includes the non-relativistic QED Hamiltonian in the dipole approximation, phonon Hamiltonian and other environmental fields, for a derivation of the master equation in the weak coupling stochastic limit see [55] and also [56, 57].

We consider one sub-unit of the trimer which consists of seven bacteriochlorophyll sites $\{1, 2, \dots, 7\}$ transferring energetic excitations from a photon-receiving antenna to a reaction center, see Fig.1.

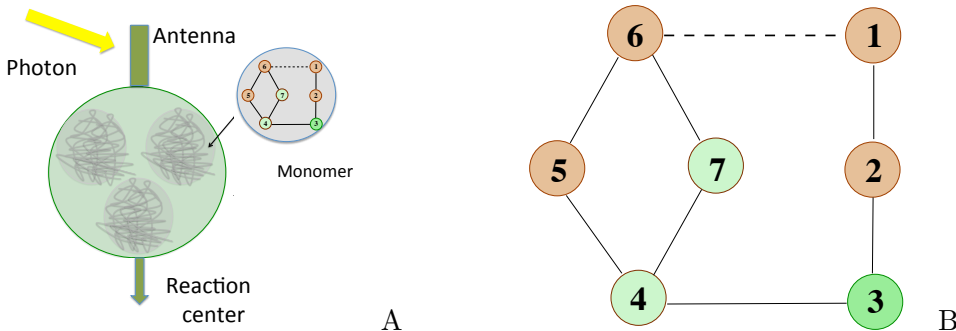


Figure 1. The schematic picture of the FMO complex. A. The FMO complex trimer. B. The schematic picture for one monomer.

¹Recently, an additional bacteriochlorophyll (the eighth) pigment was discovered in each subunit of this trimer[54].

2.1.2 Master equation

We consider the nine-state model [49, 50] for excitation transfer in the single excitation approximation which is described by a 9-dimensional subspace in the Hilbert space $(\mathbb{C}^2)^{\otimes 8}$. The possible states for the exciton will be expressed in the site basis $\{|m\rangle\}_{m=1}^7$ where the state $|m\rangle$ indicates that the excitation is present at site m . There are also a ground state $|G\rangle$ corresponding to the loss or recombination of the excitation and a sink state $|S\rangle$ corresponding to the trapping of the exciton at the reaction center (there is a discussion of the "local" and "global" bases in theory of open quantum systems in [58]). The density operator for this quantum system has the following representation in the site basis:

$$\rho = \sum_{m,n \in \{G,1,\dots,7,S\}} \rho_{m,n} |m\rangle\langle n| \quad (2.1)$$

It is assumed that the density matrix satisfies the GKS-Lindblad master equation of the following form

$$\frac{d}{dt}\rho = -i[H, \rho] + \mathcal{L}(\rho) \quad (2.2)$$

Here the Hamiltonian H describes the coupling between the seven sites states $|1\rangle, \dots, |7\rangle$:

$$H = \sum_m E_m |m\rangle\langle m| + \sum_{m < n} V_{mn} (|m\rangle\langle n| + |n\rangle\langle m|), \quad (2.3)$$

where E_m is the energy of the site m and V_{mn} describes the coupling between sites m and n . A Lindblad superoperator $\mathcal{L}(\rho)$ has the general form

$$\mathcal{L}(\rho) = \sum_m \gamma_m (2L_m \rho L_m^\dagger - \{L_m^\dagger L_m, \rho\}), \quad (2.4)$$

where L_m are arbitrary operators and γ_m are positive constants, see for example [34]. In our case for the FMO complex the Lindblad superoperator is taken in the form [47–50]

$$\mathcal{L}(\rho) = \mathcal{L}_{\text{diss}}(\rho) + \mathcal{L}_{\text{deph}}(\rho) + \mathcal{L}_{\text{sink}}(\rho) \quad (2.5)$$

Here the first term $\mathcal{L}_{\text{diss}}(\rho)$ describes the dissipative recombination of the exciton,

$$\mathcal{L}_{\text{diss}}(\rho) = \sum_m \Gamma_m (2|G\rangle\langle m| \rho |m\rangle\langle G| - \{|m\rangle\langle m|, \rho\}) \quad (2.6)$$

where Γ_m is the rate of the recombination at site m .

The second Lindblad superoperator $\mathcal{L}_{\text{deph}}$ accounts for the dephasing interaction with the environment,

$$\mathcal{L}_{\text{deph}}(\rho) = \sum_m \lambda_m (2|m\rangle\langle m| \rho |m\rangle\langle m| - \{|m\rangle\langle m|, \rho\}) \quad (2.7)$$

where λ_m is the rate of dephasing at site m .

The final term $\mathcal{L}_{\text{sink}}(\rho)$ accounts for the trapping of the exciton in the reaction center:

$$\mathcal{L}_{\text{sink}}(\rho) = \Gamma_{\text{sink}} (2|S\rangle\langle 3| \rho |3\rangle\langle S| - \{|3\rangle\langle 3|, \rho\}) \quad (2.8)$$

It is supposed that the initial state of the FMO complex is a pure excitation at site one or site six, or a mixture of these two states.

2.1.3 Entropy of entanglement and mutual information

Let two parties A and B share a quantum state ρ_{AB} in a Hilbert space $\mathcal{H}_A \otimes \mathcal{H}_B$. The von Neumann entropy of this state is

$$S(AB) = -\text{tr}(\rho_{AB} \log \rho_{AB}) \quad (2.9)$$

Similarly, one can define the entanglement entropies

$$S(A) = -\text{tr}(\rho_A \log \rho_A), \quad S(B) = -\text{tr}(\rho_B \log \rho_B), \quad (2.10)$$

where the reduced density matrices $\rho_A = \text{tr}_B \rho_{AB}$ and $\rho_B = \text{tr}_A \rho_{AB}$.

The quantum mutual information $I(A; B)$ measures the correlations shared between the two parties,

$$I(A; B) = S(A) + S(B) - S(AB). \quad (2.11)$$

This can be written as a relative entropy and is therefore non-negative:

$$I(A; B) = S(\rho_{AB} || \rho_A \otimes \rho_B) \geq 0 \quad (2.12)$$

where

$$S(\rho || \sigma) = \text{Tr}(\rho \log \rho) - \text{Tr}(\rho \log \sigma),$$

see for example [34].

Several simulations of the quantum mutual information as a function of time at cryogenic ($77^\circ K$) and physiological ($300^\circ K$) temperatures were conducted in [50]. In particular the simulations calculate the quantum mutual information with respect to several "bipartite cuts" of the sites in the FMO complex. The different cases are as follows, (Figs.1-6 in [50]):

1. The first cut was picked up where system A consists of site three and system B consists of sites one and six, (Figs.1 and 2 in [50]). Remind that the initial state of the complex is at site one, six, or the mixture, and the FMO complex transfers the excitation from these initial sites to site three.

2. The next bipartite cut is with the A system consisting of sites one and two and the B system consisting of site three, (Figs.3 and 4 in [50]).

3. Finally, the third cut was the cut where system A consists of site three and system B consists of all other sites, (Figs.5 and 6 in [50]). The quantum mutual information for this case should be larger than for the case of the other cuts.

2.1.4 Reductions of the FMO complex

We start from Fig.1. Several reductions of this system to more simple ones are considered. Some of them are schematically presented in Fig.2–Fig.4.

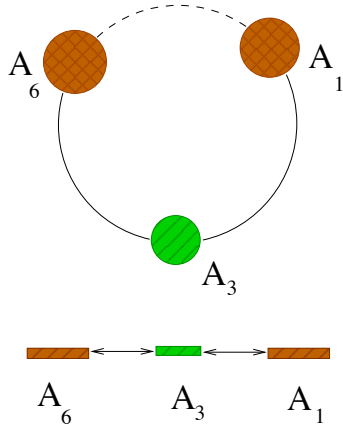


Figure 2. Schematic picture of $(1, 6|3)$ reduced FMO system.

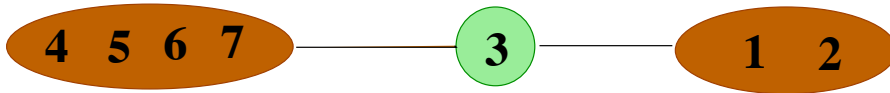


Figure 3. $(1, 2, 4, 5, 6, 7|3)$ reduction of the FMO-complex



Figure 4. $(1, 2, 5, 6|3, 4, 7)$ reduction of the FMO-complex

2.2 Holographic entanglement entropy

2.2.1 Static AdS background

Consider a quantum field theory on a d -dimensional manifold $\mathbb{R} \times \mathbb{R}^{d-1}$, where \mathbb{R} and \mathbb{R}^{d-1} denote the time axis and the $(d-1)$ -dimensional space-like manifold, respectively. Let be given a $(d-1)$ -dimensional submanifold $A \subset \mathbb{R}^{d-1}$ at fixed time $t = t_0$ and let ∂A be its boundary. Then the formula for the holographic entanglement entropy S_A in a CFT on $\mathbb{R} \times \mathbb{R}^{d-1}$ reads [7]

$$S_A = \frac{\mathcal{A}(\gamma_A)}{4G_N^{(d+1)}}, \quad (2.13)$$

where $\mathcal{A}(\gamma_A)$ is the area of γ_A , that is the $d - 1$ dimensional static minimal surface in AdS_{d+1} with metric

$$ds^2 = \frac{R^2}{z^2} \left(dz^2 - dt^2 + \sum_{i=1}^{d-1} dx_i^2 \right), \quad (2.14)$$

whose boundary is given by ∂A , and $G_N^{(d+1)}$ is the $d + 1$ dimensional Newton constant, R is the radius of AdS_{d+1} .

The simplest example for the shape of A is a straight belt at the boundary $z = 0$, see Fig.5,

$$A = \{x_i | x_1 \in [-l, l], x_{2,3,\dots,d-1} \in (-\infty, \infty)\}. \quad (2.15)$$

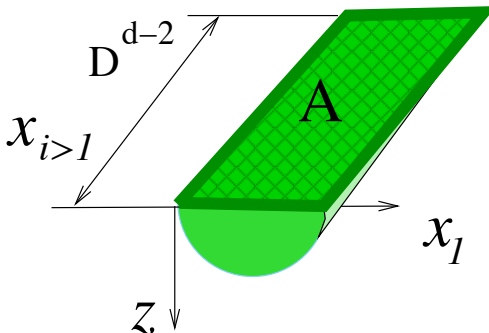


Figure 5. The standard holographic picture of a strip configuration in three spacetime dimensions at a constant time slice. ℓ is the width of the belt and $D \gg \ell$. The bulk surface extended in the direction z ends on the entanglement surface A .

In this case the area of the minimal surface, divided on the suitable constants, is [7]

$$\frac{\mathcal{A}_{vac,reg}}{R^{d-1}D^{d-2}} = \left(\frac{1}{(d-2)\epsilon^{d-2}} - \frac{c_0}{\ell^{d-2}} \right), \quad d > 2, \quad (2.16)$$

where D is the length of A in the traversal $x_{2,3,\dots,d-1}$ -direction, $\epsilon > 0$ is the UV regularization, c_0 is a positive constant depending on d . The first term is divergent when $\epsilon \rightarrow 0$, but for our purpose it will not play a role, since we will consider the differences of entanglement entropies.

For an excited state whose gravitational dual is provided by the black brane solution with mass m and the Hawking temperature $T_H = dm^{1/d}/4\pi$ (here we assume $R = 1$)

$$ds^2 = \frac{1}{z^2} \left(-f(z)dt^2 + \frac{dz^2}{f(z)} + \sum_{i=1}^{d-1} dx_i^2 \right), \quad f(z) = 1 - mz^d, \quad (2.17)$$

in general, it is not possible to find an explicit expression for the entanglement entropy for $d > 3$. It can be found from the integral equation relating the entropy to an auxiliary

parameter z_*

$$\frac{\mathcal{A}_{exc,ren}}{2R^{d-1}D^{d-2}} = \frac{1}{z_*^{d-2}} \int_0^1 \frac{dw}{w^{d-1}} \left[\frac{1}{\sqrt{f(z_*w)(1-w^{2(d-1)})}} - 1 \right] - \frac{1}{(d-2)z_*^{d-2}}, \quad (2.18)$$

meanwhile the parameter z_* is related to the width of the belt

$$\frac{\ell}{2} = z_* \int_0^1 \frac{w^{2(d-1)} dw}{\sqrt{f(z_*w)(1-w^{2(d-1)})}}.$$

2.2.2 Time dependent AdS Vaidya background

The proposal (2.13) has been generalized to time dependent geometries in [10]. In the Vaidya AdS $_{d+1}$ spacetime the corresponding minimal surface describes the thermalization process in the d-dimensional boundary theory [14], see also [12, 13, 17]. The Vaidya AdS $_{d+1}$ metric has the form

$$ds^2 = \frac{R^2}{z^2} \left(-f(v, z) dv^2 - dv dz + \sum_{i=1}^{d-1} dx_i^2 \right), \quad (2.19)$$

where the function

$$f(v, z) = 1 - m(v)z^d. \quad (2.20)$$

The form of $m(v)$ is usually chosen to be

$$m(v) = \frac{m}{2} \left(1 + \tanh \frac{v}{\alpha} \right) \quad (2.21)$$

The metric (2.19) with this function describes a spacetime model which evolves from pure AdS at early times to the Schwarzschild black brane at late times because of the shell of null dust infalling along $v = 0$. The parameter α determines the thickness of the shell. The case $\alpha \rightarrow 0$ corresponds to a step function and one deals with a shock wave.

We will consider also the shell in the AdS $_{d+1}$ black brane background (the Vaidya AdS black brane metric), in this case

$$m(v) = m_0 + \frac{m}{2} \left(1 + \tanh \frac{v}{\alpha} \right) \quad (2.22)$$

The entanglement entropy is given by the extremum of the functional [14, 17]

$$\frac{\mathcal{A}}{2R^{d-1}D^{d-2}} = \int_0^\ell \frac{dx}{z^{d-1}} \sqrt{1 - [1 - m(v)z^d](v')^2 - 2v'z'}, \quad (2.23)$$

where $z = z(x)$, $v = v(x)$ and $v' = dv/dx$.

The Euler-Lagrange equations corresponding to the action (2.23) read

$$[1 - m(v)z^d]v'' + z'' - \frac{\partial_v m(v)}{2} z^d (v')^2 - d m(v) z^{d-1} z' v' = 0, \quad (2.24)$$

$$z v'' - \frac{d-2}{2} m(v) z^d (v')^2 + (d-1)[(v')^2 + 2v'z' - 1] = 0. \quad (2.25)$$

For the system of equations (2.24), (2.25) we will solve numerically the Cauchy problem with initial data (2.27), (2.27)

$$z(0) = z_*, \quad v(0) = v_*, \quad (2.26)$$

$$z'(0) = v'(0) = 0, \quad (2.27)$$

We are interested in finding solutions that reach the boundary at some point, that we identify² with ℓ in (2.23) at the boundary time t :

$$z(\ell) = 0, \quad v(\ell) = t. \quad (2.28)$$

Equations (2.24), (2.25) have an integral of motion

$$\left(\frac{z_*}{z}\right)^{2(d-1)} = 1 - [1 - m(v)z^d](v')^2 - 2v'z'. \quad (2.29)$$

Due to this identity the integral in (2.23) can be substantially simplified to give

$$\frac{\mathcal{A}_{reg}}{2R^{d-1}D^{d-2}} = \int_0^{\ell-\epsilon} \frac{z_*^{d-1}}{z^{2(d-1)}} dx, \quad (2.30)$$

where we introduce regularization $\epsilon > 0$. This integral contains the UV divergence when $\epsilon \rightarrow 0$. The renormalized version of (2.30) can be written as [14, 17]

$$\frac{\mathcal{A}_{ren}}{2R^{d-1}D^{d-2}} = \int_0^{\ell-\epsilon} \frac{z_*^{d-1}}{z^{2(d-1)}} dx - \frac{1}{(d-2)(z(\ell-\epsilon))^{d-2}}, \quad d > 2, \quad (2.31)$$

and regularization can be removed. Note, that in the case of $d = 2$ [14, 17]

$$\frac{\mathcal{A}_{ren}}{2R} = \int_0^{\ell-\epsilon} \frac{z_*}{z^2} dx + z_* \log(z(\ell-\epsilon)). \quad (2.32)$$

It is quite straightforward to find the dependence of the renormalized entanglement entropy on z_* and v_* . To find the dependence of the entanglement entropy on ℓ and t one has to parametrize the solutions to (2.27)-(2.25), not by (z_*, v_*) , but by ℓ and t .

It happens that the values of ℓ and t are very sensitive to the initial data (2.26), and one needs a special numerical procedure to find the pair (z_*, v_*) corresponding to the given pair ℓ, t with large values of ℓ, t , see [17, 25, 28] and refs therein for more details. It is interesting to note that the case when $m_0 > 0$ in (2.22) is more stable than the case $m_0 = 0$.

In Fig.7 the dependence of the renormalized holographic entanglement entropy on t and ℓ for the propagating Vaidya shell in the four dimensional black brane background with $f = f(z, v)$ given by (2.20) and (2.22) is presented. As compare with the dependence of the holographic entanglement entropy for the Vaidya AdS₄ metric the entropy does not go to fixed value for large ℓ , but as both go to constant values for large times. The same is shown in Fig.8 for the three dimensional black brane background.

Note that the similar technique has been intensively used in study the thermalization processes, especially for non-conformal invariant backgrounds, see [25, 28, 60–62] and refs therein.

²In our calculation the width of the belt is 2ℓ , although on some pictures we omit the factor 2.

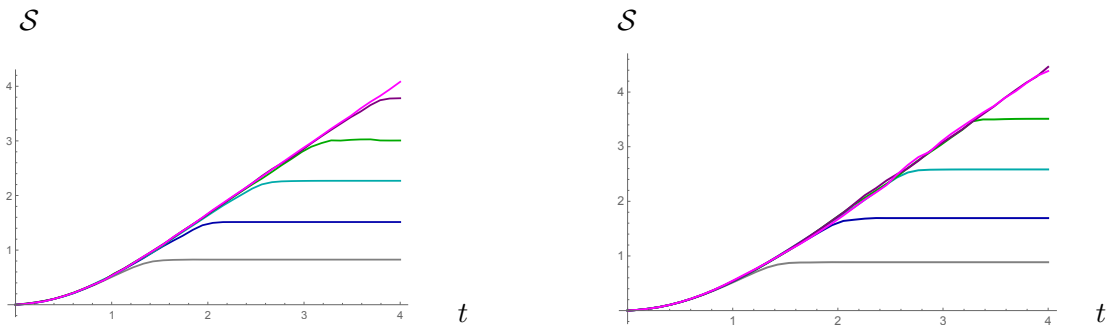


Figure 6. The time dependence of the holographic entanglement entropy $\mathcal{A}_{ren,3}(\ell, t)$, after the corresponding initial state subtraction, for the Vaidya metric in the four dimensional black brane background with $f = f(z, v)$ ($m_0 = 0.25$, $m = 1$ in the left panel and $m_0 = 0$, $m = 1$ in the right panel) at fixed $\ell = 1, 1.5, 2, 2.5, 3, 3.5$ (gray, blue, darker cyan, green, purple and magenta, respectively). For all cases $\alpha = 0.2$

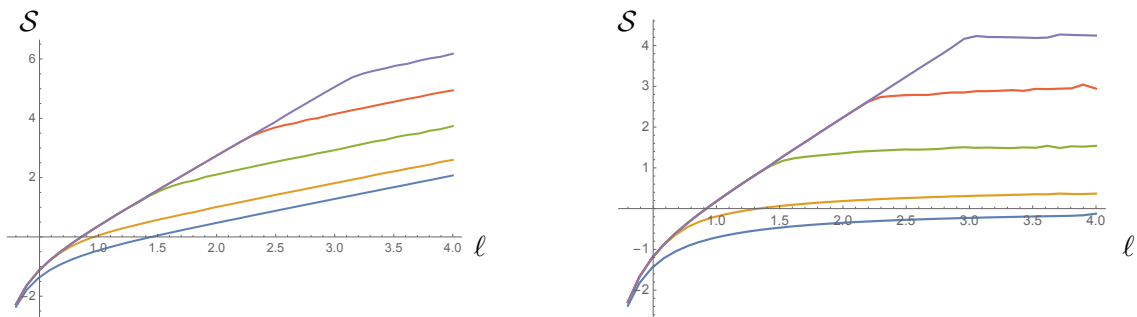


Figure 7. The renormalized holographic entanglement entropy $\mathcal{A}_{ren,3}(\ell, t)$, up to the normalizing factor, for the Vaidya metric in the four dimensional black brane background with $f = f(z, v)$ ($m_0 = 0.25$, $m = 1$ in the left panel and $m_0 = 0$, $m = 1$ in the right panel) at fixed $t = 0, 1, 2, 3, 4$ (blue, orange, green, red and darker blue, respectively) as function of ℓ . For all cases $\alpha = 0.2$

2.3 Iterative procedure to calculate $\mathcal{S}(A_1 \cup A_2 \cup \dots \cup A_n)$

In this section we present the rules that help to calculate the holographic entropy for n disjoint objects. Here we consider for illustration a particular case of n -segments. This problem has been studied in several papers [15–17, 22, 23, 31]. It is substantially simplified in the case of equal length strips and equal separation between them. However in order to deal with holographic description of the FMO complex, we have to find the entropy for non-equal length strips.

To find the entropy one has to find the global minimum among all possible configurations. To specify all possible configurations corresponding to local minimum surfaces it is convenient to use the diagrammatic language. In special cases, it happens that only primitive diagrams contribute to the entropy. The primitive diagrams are diagrams that do not contain cross-sections of the connected lines and also do not contain diagrams with

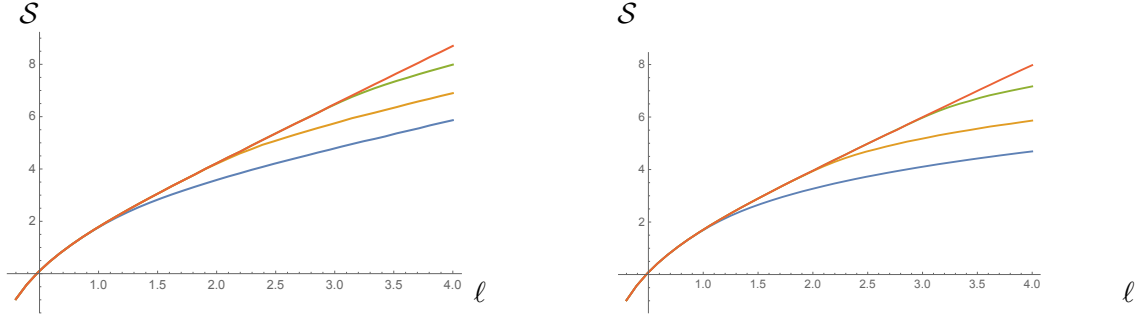


Figure 8. The renormalized holographic entanglement entropy $\mathcal{A}_{ren,2}(\ell, t)$, up to the normalizing factor, for the Vaidya metric in the three dimensional black brane background with $f = f(z, v)$ given by (2.20) and (2.22) ($m_0 = 0.25$, $m = 1$ in the left panel and $m_0 = 0$, $m = 1$ in the right panel) at fixed $t = 0, 1, 2, 3$ (blue, orange, green and red, respectively) as function of ℓ . For all cases $\alpha = 0.2$

”engulfed” sub-diagrams in the terminology used in [23]. Note that the class of primitive diagrams contains less diagram than so-called rainbow diagrams in the Boltzmann quantum field theory [63]. It is possible that for more complicated backgrounds one has to take into account more diagrams than only the primitive diagrams.

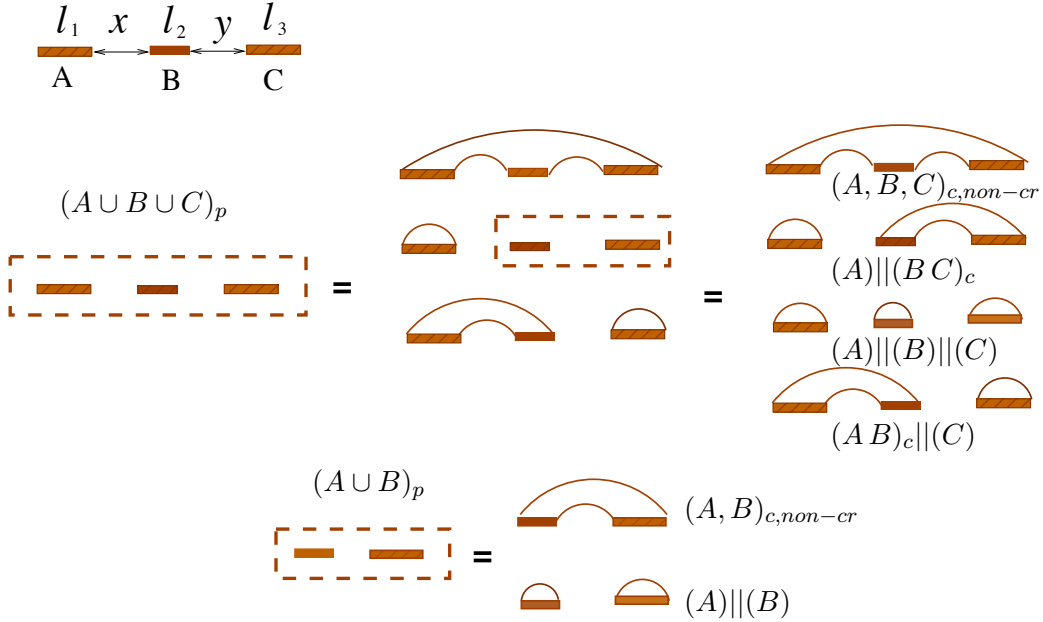


Figure 9. The decompositions (2.35) for 3 and 2 segments that include only primitive diagrams. Selections of primitive diagrams are indicated by dashed lines.

In Fig.9 we show primitive diagrams that contribute to calculation of the entanglement entropy for 2 and 3 segments. There are three competing minimal surfaces for 2 segments A and B , see Fig.17 below, one surface corresponds to a ”disjoint” configuration $(A||B)$, the second to a ”connected non-crossing” one $(A, B)_{c, non-cr}$, the third to a ”crossing” one

$(A, B)_{c,cr}$, and we can write the symbolic representation

$$(A \cup B) = (A)|| (B) + (A, B)_{c,non-cr} + (A, B)_{c,cr}, \quad (2.33)$$

here the brackets in $(A \cup B)$ mean that we deal with corresponding diagrams and in the RHS of (2.33) we list these diagrams. Due to a possible change of the leader in this competition the system may undergo a phase transition under change the geometrical parameters, see [22, 23].

For 3 segments one can write the full decomposition as

$$\begin{aligned} (A \cup B \cup C) = & (A)|| (B)|| (C) + (A, B, C)_{c,cr} \quad (2.34) \\ & + (A, B, C)_{c,non-cr} + (A, B)_c || (C) + (A)|| (B, C)_c + (A, \underbrace{\mathbf{B}}_C)_c \end{aligned}$$

The first term represents the totally disconnected diagram (the disconnected parts are separated by symbol $||$). The second and the third terms represent the crossing (“intersecting”) and non-crossing connected diagrams. The last three terms correspond to diagrams with disjoint parts, wherein the last term corresponds to the rainbow diagram. The rainbow diagram contains an “engulfed” subdiagram (in terminology used in [23]), that is indicated by writing the corresponding symbol by the bold letter \mathbf{B} and the curl underbrace bracket. We call the diagram corresponding to the first, third, fourth and fifth terms as primitive diagrams. We use the same terminology also for n -segment cases. Due to the competition between different terms in decomposition(2.34) there are phase transitions. The number of possible phases depends on number of diagrams that contribute to the entropy. For 3 segments of equal length and with unequal separations, the competition between primitive diagrams gives rise to, generally speaking, 4 phases [15–17, 22, 23]. The similar situation takes place for non-equal lengths and in Fig.10 we present the phase diagrams for $l_1 \neq l_2 \neq l_3$ and equal separations.

To calculate $\mathcal{S}(A_1 \cup A_2 \cup \dots \cup A_n)$ taking into account only the primitive diagrams we use the following representation

$$(A_1 \cup A_2 \cup \dots \cup A_n)_p = (A_1, A_2, \dots, A_n)_c + \sum_{j=1}^{n-1} (A_1, A_2, \dots, A_j)_c \star (A_{j+1} \cup A_2 \cup \dots \cup A_n)_p \quad (2.35)$$

where $(A_1, A_2, \dots, A_j)_c$ is the bulk connected surface ending on segments A_1, A_2, \dots, A_n constructed without any crossing lines. There is only one such surface for a given number of segments. In 2.35 there is the symbol \star that means that sub-diagrams on the left and on the right of the symbol compose the same n -segment diagram. We will omit this symbol in what follows. The decomposition (2.35) for 3 and 7 segments is shown in Fig. 9 and Fig. 12, respectively (or the moment, the reader can ignore the different colors for segments and connecting lines in Fig.12). In these pictures contributions to $(A_1 \cup A_2 \cup \dots \cup A_n)_p$ are shown by the enveloping rectangles.

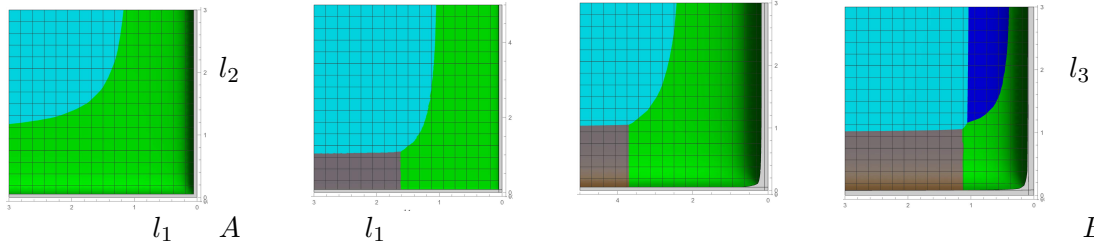


Figure 10. **A.** The phase diagrams for 2 strips, A, B with unequal lengths l_1, l_2 . The green color regions correspond to the bulk surface $(A)|| (B)$, the cyan color regions correspond to the bulk surface $(A, B)_c$, **B.** The phase diagrams for 3 strips, A, B, C , with unequal lengths l_1, l_2, l_3 . The green color regions correspond to the bulk surface $(A)|| (B)|| (C)$, the blue color regions correspond to the bulk surface $(A)|| (BC)_c$, the gray color regions correspond to the bulk surface $(AB)_c|| (C)$ and the cyan color corresponds to the bulk surface $(A, B, C)_{c, non-cr}$. Different colors regions are separated by the curves that are the transition lines. In the left plot $l_1 = l_2$, in the middle plot $l_2 = 0.3l_1$ and in the right plot $l_2 = 3l_1$ and we vary l_1 and l_2 keeping the distances between segments fixed. All plots correspond to AdS_4 .

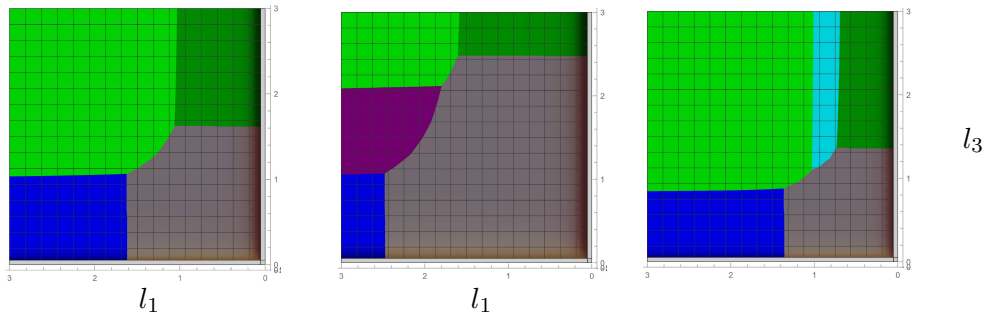


Figure 11. The phase diagrams for 4 strips, A_1, A_2, A_3, A_4 with unequal lengths l_1, l_2, l_3, l_4 . The gray color regions correspond to the bulk surface $(A_1)|| (A_2)|| (A_3)|| (A_4)$, the green color regions correspond to the bulk surface $(A_1, A_2, A_3, A_4)_{c, non-cr}$, the cyan color regions correspond to the bulk surface $(A_1)|| (A_2 A_3 A_4)_c$ and the purple color corresponds to the bulk surface $(A_1 A_2 A_3)_c|| (A_4)$. Dark green and dark blue regions correspond to the bulk surface $(A_1)(A_2)|| (A_3 A_4)_c$ and $(A_1, A_2)_c|| (A_3)(A_4)$, respectively. Different colors regions are separated by the curves that are the transition lines. In the left plot $l_1 = l_2, l_3 = l_4$, in the middle plot $l_2 = 0.5l_1, l_4 = 0.5l_3$ and in the right plot $l_2 = 1.5l_1, l_4 = 1.5l_3$ and we vary l_1 and l_2 keeping the distances between segments fixed. All plots correspond to AdS_4 .

To calculate $\mathcal{S}(A_1 \cup A_2 \cup \dots \cup A_n)$ taking into account also the Boltzmann rainbow diagrams one can use the following representation

$$(A_1 \cup A_2 \cup \dots \cup A_n)_B = (A_1, A_2, \dots, A_n)_{cwB} + \sum_{j=1}^{n-1} (A_1, A_2, \dots, A_j)_{cwB} \star (A_{j+1} \cup A_2 \cup \dots \cup A_n)_B \quad (2.36)$$

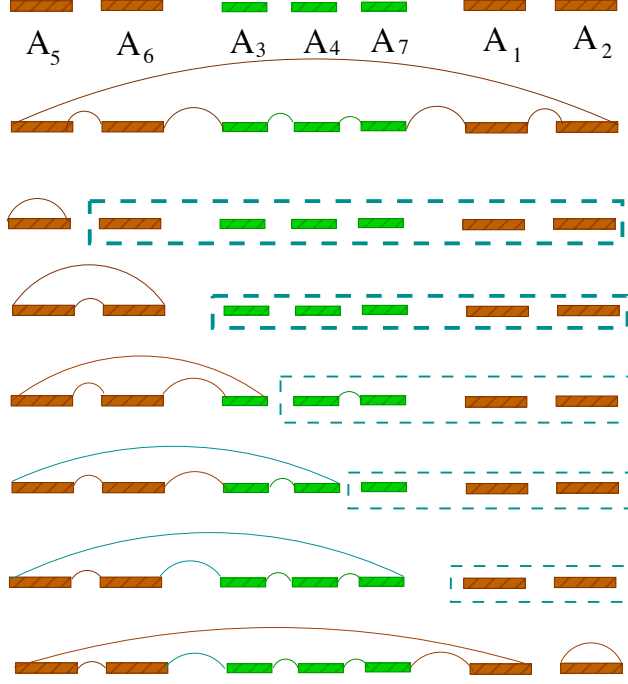


Figure 12. Recursive procedure (2.35) to calculate $(A_5 \cup A_6 \cup A_3 \cup A_4 \cup A_7 \cup A_1 \cup A_2)_p$

where $(A_1, A_2, \dots, A_n)_{cwB}$ are connected diagrams with Boltzmann insertions,

$$\begin{aligned}
(A_1, A_2, \dots, A_j)_{cwB} = & \sum_{\substack{\{i_q\}, \{k_q\} \\ \sum_{q=1}^l (i_q + k_q) \leq j-2}} \left(A_1, \dots, A_{i_1}, \underbrace{(A_{i_1+1} \cup A_{i_1+2} \cup \dots \cup A_{i_1+k_1})}_B A_{i_1+k_1+1}, \dots \right. \\
& A_{i_1+i_2+k_1}, \underbrace{(A_{i_1+i_2+k_1+1} \cup A_{i_1+i_2+k_1+2} \cup \dots \cup A_{i_1+i_2+k_1+k_2})}_B A_{i_1+i_2+k_1+k_2+1}, \dots, \\
& \left. \underbrace{A_{1+\sum_{q=1}^l i_q + \sum_{q=1}^{l-1} k_q} \cup \dots \cup A_{\sum_{q=1}^l (i_q + k_q)}}_B A_{1+\sum_{q=1}^l (i_q + k_q)}, \dots, A_j \right)_c
\end{aligned} \tag{2.37}$$

Here the Boltzmann insertions are indicated by the bold letters and curl underbrace brackets. Note, that cwB diagrams are not connected, but if we remove the Boltzmann insertions we are left with the connected diagrams. In particular, if we remove the Boltzmann insertions in the RHS of (2.37) we left with connected diagrams

$$(A_1, \dots, A_{i_1}, A_{i_1+k_1+1}, \dots, A_{i_1+i_2+k_1}, A_{i_1+i_2+k_1+k_2+1}, A_{1+\sum_{q=1}^l (i_q + k_q)}, \dots, A_j)_c$$

Comparing (2.35) with (2.36) and (2.37) we see that the Boltzmann diagrams are composed by insertions of low order Boltzmann diagrams to primitive diagrams.

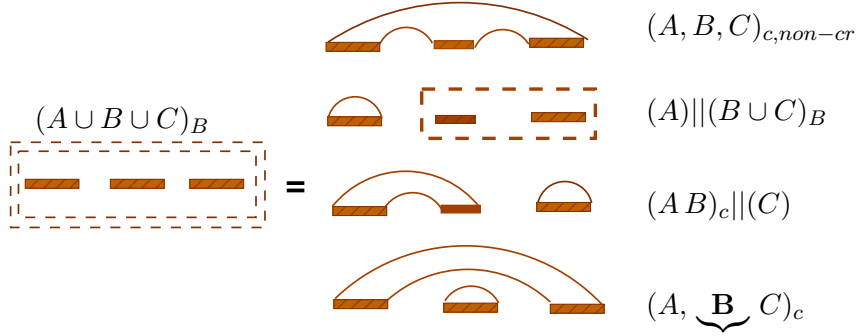


Figure 13. The decomposition (2.37) for 3 segments. Selections of Boltzmann diagrams are indicated by double dashed lines. There are no difference between the primitive and the Boltzmann selections for two segments, but there is the difference for 3 and more segments.

2.4 Holographic mutual information

The mutual information $I(A; B)$ of two entangling regions A and B is defined by (2.11):

$$I(A; B) = S(A) + S(B) - S(A \cup B), \quad (2.38)$$

where $S(A \cup B)$ is the entropy of the union of two regions. Holographic definition of the mutual information $I(A; B)$ just means that we calculate all terms in the RHS of (2.39) holographically.

To find $S(A \cup B)$ one has to find the minimal surface between two competing ones, "joint" and "disjoint" surfaces, as shown in Fig.17. The winner, in the case of vacuum background, depends only on the ratios of segments to the distance between them. It is obvious that $I(A; B)$ is equal to zero for the case when the minimal surface is realized on the "disjoint" configuration. Generally speaking, $I(A, B)$ undergoes a first order phase transition as one increases the distance between two strips [9, 11, 19]

$$I(A; B) = \begin{cases} \mathcal{I}(A; B), & \text{if } \mathcal{I}(A; B) \geq 0 \\ 0 & \text{if } \mathcal{I}(A; B) \leq 0 \end{cases} \quad (2.39)$$

$$\mathcal{I}(A; B) \equiv S(A) + S(B) - S(A + x + B) - S(x), \quad (2.40)$$

where $S(A)$ are areas of surfaces entangling the belt (stript) with segment A . In the case of the AdS_d background $\mathcal{I}(A; B)$ is given by

$$\frac{\mathcal{I}(A; B)_{vac}}{2L^{d-2}c_0} = -\frac{1}{\ell_1^{d-2}} - \frac{1}{l_1^{d-2}} + \frac{1}{(\ell_1 + \ell_2 + x)^{d-2}} + \frac{1}{x^{d-2}}, \quad (2.41)$$

here $d > 2$. The region where the mutual information is nonzero depends on the ratios of parameters $\ell_1/x, \ell_2/x$ in the case of AdS_d , and on the ratios of parameters $\ell_1/x, \ell_2/x$ and $z_h/x, z_h = m^{-1/d}$, in the case of AdS_d black brane, see 14 and Fig.15. From these plots we clearly see that the mutual information of two static belts is maximal when the system is in the vacuum state.

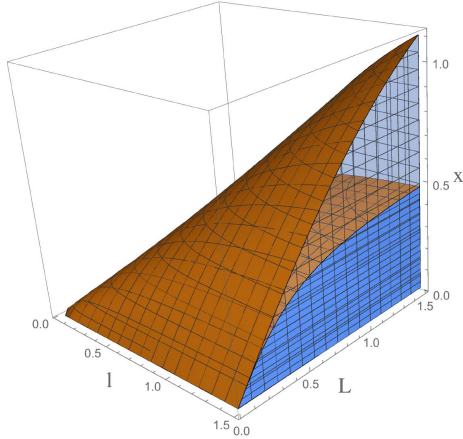


Figure 14. The regions of non-zero holographic mutual information for two strips with the widths ℓ and L and distance x for two thermal states whose gravity duals are given by the AdS_4 black brane metric (2.17) with $m = 0.25$ and $m = 1$. The region corresponding to $m = 1$ is inside the region corresponding to $m = 0.25$

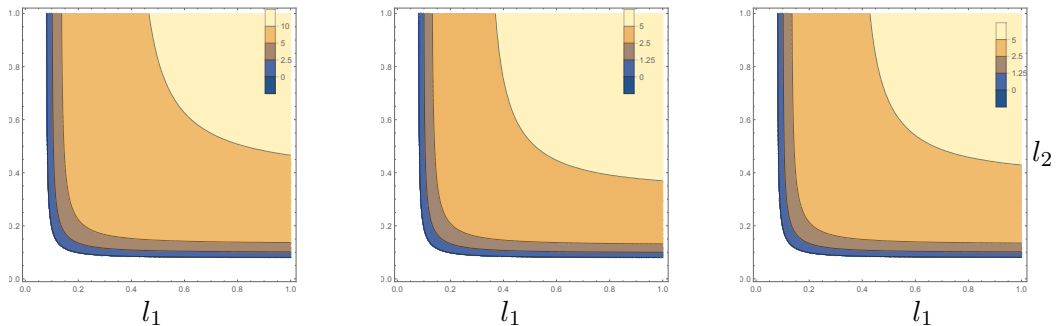


Figure 15. The density plots of the holographic mutual information for two strips with the widths ℓ_1 and ℓ_2 and fixed distance $x = 0.08$ for the static vacuum state whose gravity dual is the AdS_4 metric (the left plot) and two thermal states whose gravity duals are provided by the AdS_4 black brane metric (2.17) with $m = 0.25$ and $m = 1$, respectively (the middle and the right plots)

3 Holographic studies of simplest FMO complex

3.1 Holographic entanglement entropy for two site system during a quench at nonzero temperature.

As has been mention in Sect.2.1.4, the simplest model of LHC is the two systems model. We can consider two parallel infinite strips with non-equal widths $2\ell_1$ and $2\ell_2$ separated by

a distance $2x$ in a d -dimensional field theory as depicted in Fig.16 as a simplest model of LHC and find the mutual information induced by the coming photon. This coming photon we model by the Vaidya shell.

The holographic mutual information for two parallel strips in static backgrounds and in the Vadya AdS has been studied in several papers [10, 15–17, 22, 30]. In particular for equal widths of segment in certain limits the analytical results have been obtained [22]. The specificity of our consideration here is that we want to consider the time dependence of the mutual information during a global quench of a medium that already has high temperature. The corresponding holographical model is given by the Vaidya shell propagating in the AdS_{d+1} black brane background. We also compare the obtained time dependence with the time dependence of the thermalization process started from the zero temperature.

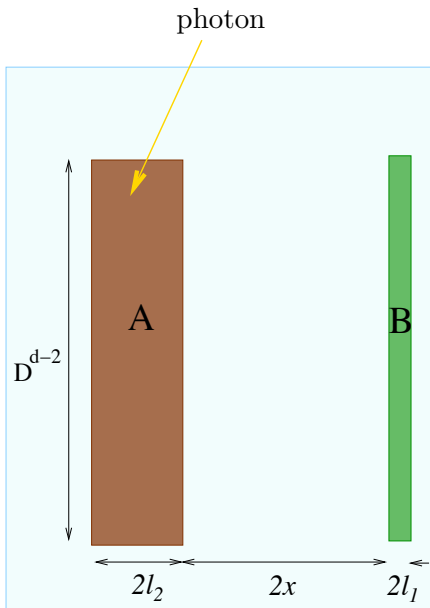


Figure 16. Schematic picture of locations of the excited complex (A) and the out site (B), that sends the information to the reaction center, and the infalling photon.

As already has been mentioned in Sect.2.3, equation 2.33, given the two disconnected regions A and B in the boundary, there are three configurations of hypersurfaces extending in the bulk whose boundaries coincide with $\partial(A \cup B) = \partial A \cup \partial B$: the “disjoint” configuration, the “connected” configuration, given by a bridge connecting A and B through the bulk and the “crossing” configuration, that looks as a configuration with cross-sections in the projection on the (x, z) -plane, Fig.17. The “crossing” configurations do not contribute to the holographic entropy calculations [22, 23], in the static AdS and AdS black brane backgrounds. They also do not contribute to the same calculations during the thermalization process described by the Vaidya AdS metric [17]. We have checked numerically that they do not contribute in the case of the Vaidya AdS black brane metric during the transition from the black brane with mass m_0 to the black brane with mass $m_0 + m$, see cartoon plots in Fig.18. In these plots we show the leading contributions to the entangle-

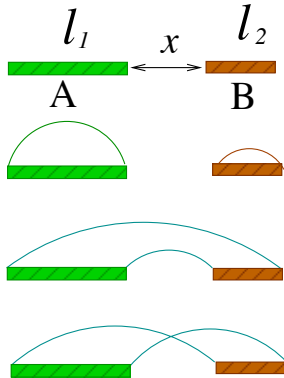


Figure 17. Illustration of bulk surfaces anchored to the boundaries of disjoint regions A and B. The surfaces started and ended on the boundaries of the same region are shown by the same color as the region, meanwhile the surfaces connecting the ends of different regions are shown by blue lines. In the case of considered here holographic models we do not obligate to take into account the diagram with crossing lines depicted in the last line.

ment entropy for 2 strips, A and B , with unequal lengths l_1, l_2 , at different times during the transition from the black brane configuration with the small mass m_0 to the large mass m in AdS_3 . The green color regions correspond to the bulk surface $(A)||_c(B)$, the blue color regions correspond to the bulk surface $(BC)_c$. In our program we have used the red color to indicate contribution of the bulk surface $(AB)_{c,cr}$, but we have not seen red regions for all variety of parameters $0.2 < l_1, l_2, x < 1.5$, $0 < t < 4$. Transition lines separate the different color region and as usual are interpreted as the lines of topological phase transitions. Note that one can solve this problem analytically for the case of infinitely thin shell in AdS_3 black brane.

3.2 Holographic mutual information for two site system at nonzero temperature.

Let us first consider the holographic mutual information $S(A \cup B)$ for the Vaidya shell in the three dimensional AdS black brane background with $f = f(z, v)$ given by (2.20) and (2.22), and two segments shown in Fig.17, as function of the boundary time t at fixed l_1, l_2, x . This quantity depends on many parameters, l_1, l_2, x, m, m_0 and α and we perform our analysis numerically. On the right in Fig.17 we show the case $m_0 = 0.25$ and on the left we show for comparison the case $m_0 = 0$ considered before in [16, 17]. The same color curves correspond to the same fixed values of l_1 and x , herewith different style lines (solid, dashed and dotted) correspond to different values of l_2 for both cases, $m_0 = 0.25$ and $m_0 = 0$.

We see that some color and style lines present in both, left and right plots in Fig.19, but some color and style lines present only in the left plot in Fig.19. In particular, there are no purple lines in Fig.19.B. Notice that the character of time dependences shown in the left and right plots are the same. There are curves that start from non-zero value of the mutual

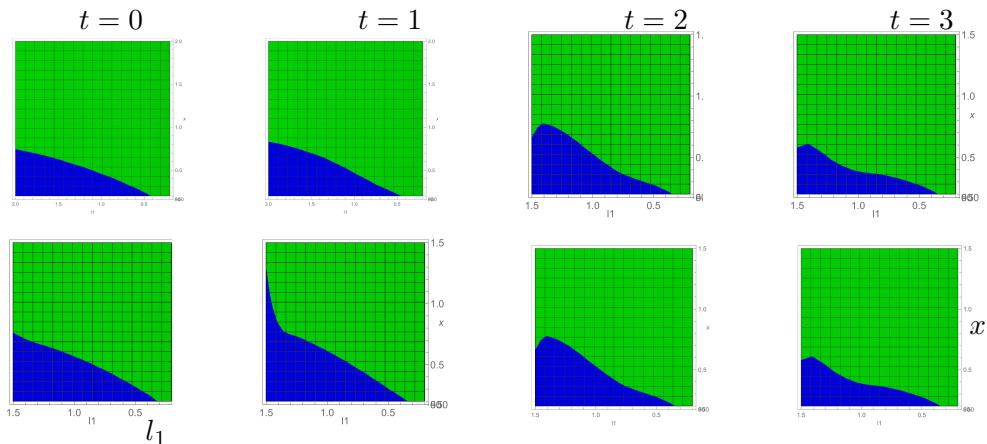


Figure 18. Cartoon diagrams that show contributions of various diagrams to the entanglement entropy for 2 strips, A and B , with unequal lengths l_1, l_2 , at different times during the transition from the black brane configuration with the small mass m_0 to the large mass m in AdS_3 . The green color regions correspond to the bulk surface $(A)|(B)$, the blue color regions correspond to the bulk surface $(BC)_c$, the red color regions correspond to the bulk surface $(AB)_{c,cr}$ (we do not see red regions). Different colors regions are separated by the curves that are the transition lines. In the top plots $l_2 = l_1$, and $t = 0, 1, 2, 3$, in the bottom plots $l_2 = 2l_1$, and we vary l_1 and x . All plots correspond to $\alpha = 0.2$.

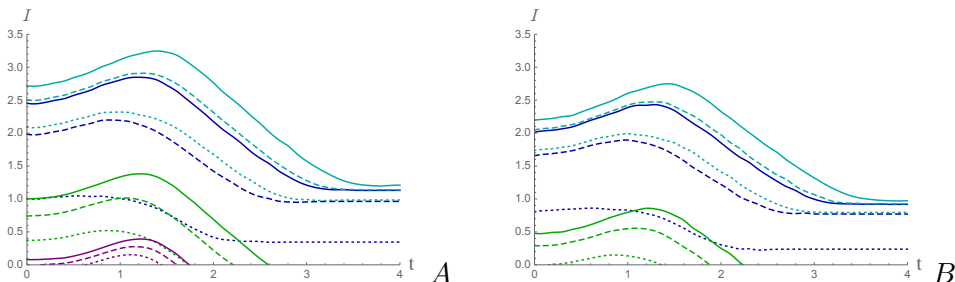


Figure 19. Holographic mutual information $I(A, B)$, up to the normalizing factor, for the Vaidya metric in the three dimensional black brane background with $f = f(z, v)$ given by (2.20) and (2.22) ($m_0 = 0, m = 1$ for the panel **A** and $m_0 = 0.25, m = 1$ for the panel **B**) and two segments shown in Fig.17, as function of the boundary time t at fixed l_1, l_2, x . The same color curves are characterized by fixed values of l_1 and x and varying l_2 . Blue lines correspond to $l_1 = 1.5$ and $x = 0.2$ and solid, dashed and dotted styles correspond to $l_2 = 1.5, 1$ and 0.5 , respectively; green lines correspond to $l_1 = 1.5$ and $x = 0.4$ and solid, dashed and dotted styles correspond to $l_2 = 1.5, 1.2$ and 0.9 , respectively; purple lines correspond to $l_1 = 1.5$ and $x = 0.6$ and solid, dashed and dotted lines correspond to $l_2 = 1.5, 1.4, 1.3$; dark cyan lines correspond to $l_1 = 1.7$ and $x = 0.2$ and solid, dashed and dotted lines correspond to $l_2 = 1.5, 1.2, 0.9$. For all cases $\alpha = 0.2$. We see that there are no purple lines in plots B.

information I_0 , then increase during some time t_{max} up to some maximal value, I_{max} and then during the saturation time t_s go to other constant value I_s . Increasing the starting

temperature we decrease the corresponding t_r and t_s . There are also curves that start from $I_0 \neq 0$, reach I_{max} and then at the scrambling time t_{sc} become zero. At the scrambling time any sort of correlations, in particular the exchange of information, is erased. There is also the regime when the mutual information starts from zero at wake up time, t_{wu} , then it increases up to the maximum and when becomes zero at $t = t_{sc}$. In this regime the time dependence has the bell form and it is more interesting for us, see Sect.3.3. There are also geometrical configurations, when I is zero at all times. These configurations correspond to the cases with large distances x .

The time dependence, in the logarithmic time scale, of the holographic mutual information $S(A \cup B)$ for the Vaidya shell in the four dimensional AdS black brane background is presented in Fig.20. Comparing Fig.20 and Fig.19 we see that the qualitative features of the curves are the same.

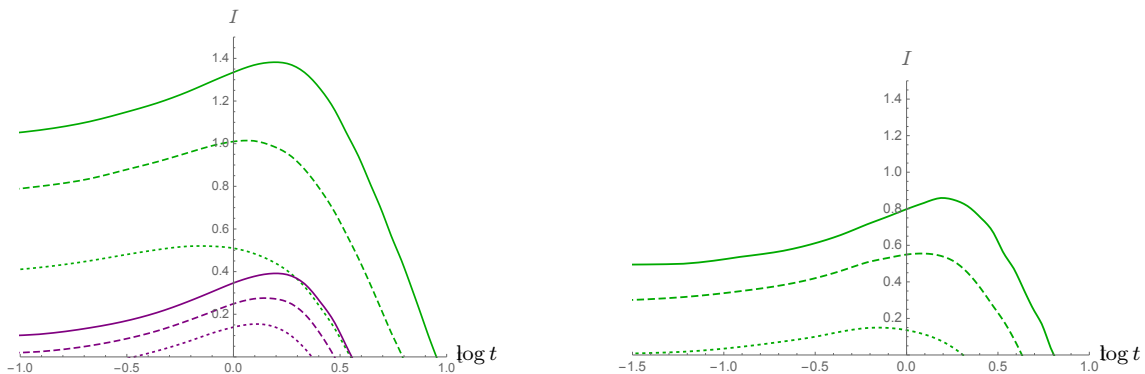


Figure 20. Holographic mutual information $I(A, B)$, up to the normalizing factor, for the Vaidya metric in the four dimensional black brane background with $f = f(z, v)$ given by (2.20) and (2.22) ($m_0 = 0, m = 1$ for the left panel and $m_0 = 0.25, m = 1$ for the right panel) and two belts shown in Fig.16, as function of the boundary time t (in the logarithmical scale) at fixed l_1, l_2 and x . The same color curves are characterized by fixed values of l_1 and x and varying l_2 . For all green lines $l_1 = 1.5, x = 0.2$ and the solid, dashed and dotted green lines correspond to $l_2 = 1.5, 1.2, 0.9$, respectively; for all purple lines $l_1 = 1.5, x = 0.6$ and the solid, dashed and dotted purple lines correspond to $l_2 = 1.5, 1.4, 1.3$, respectively. For all cases $\alpha = 0.2$

3.3 Matching holographic calculations to the simulation results.

It is obvious that we find the scaling behavior of the holographic mutual information only up to normalization factors. To fit the mutual information for a given physical system there are 3 numerical parameters in our disposal: the $(d+1)$ - dimensional gravity constant, the radius of the AdS and the scale, that in our case can be identified with the black brane mass. We compare the results of our calculations with the mutual information $I(A; B)$ calculated for the reduced FMO system in [50], where system A consists of site three and system B consists of site one, see Fig.3a in [50]. We reproduce this curve in Fig.21 by the purple dashed line. In Fig.4a of [50] this quantity at physiological temperature (300°K) is presented. We reproduce this curve in Fig.21 by the red dashed line. We see that in this

particular case the purple curve has a maximum approximately twice higher when the red one. As it is shown in Fig.21 these two curves fit two curves that we take from Fig.20 for particular choices of the geometry of two strips.

It is interesting to note, that the mutual information calculated in [50] for the the reduced FMO system, where system A consists of site three and system B consists of site six, or two, see Fig.1b and 3b in [50], has the two-humped form. We can reproduce this form of the time dependence of the mutual information taking two thin shells Vaidya AdS_{d+1} metric with

$$m(v) = \frac{m_1}{2} \left(1 + \tanh \frac{v}{\alpha} \right) + \frac{m_2}{2} \left(1 + \tanh \frac{v - v_0}{\alpha} \right), \quad (3.1)$$

cf.[59].

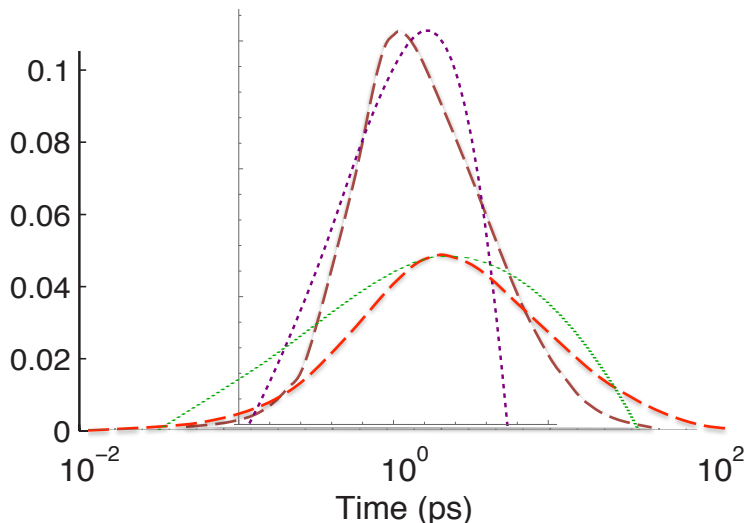


Figure 21. The purple and red dashed lines show the time dependence of the mutual information of the reduced FMO system calculated in [50] at 70°K and 300°K temperature, respectively. The green and purple solid lines show the rescaled time dependence of the holographical mutual information presented in Fig.20 for the cases of the global quench in AdS₄ and AdS₄ black brane, respectively.

3.4 Wake up and scrambling times

As we have seen in Sect.3.2 there are configurations for which the time dependence of the mutual information has the bell form, see also plots in Fig.22. We see that for some time the mutual information is equal to zero (or very small) then at the wake up time t_{wu} it starts to increase, reaches the maximum at time t_{max} and then decreases and vanishes at the scrambling time t_{scr} . This behaviour can be explained by a causality argument [16]. It is supposed that before the quench there is a finite correlation length in the system. Therefore after the quench only excitations created at nearest points will be entangled. At later times, such entangled pairs will only contribute to the mutual information between two intervals, if each interval contains one of the two particles.

The scrambling time is the time scale at which all correlations in a system have been destroyed after introducing a perturbation [30]. One defines the scrambling time as the

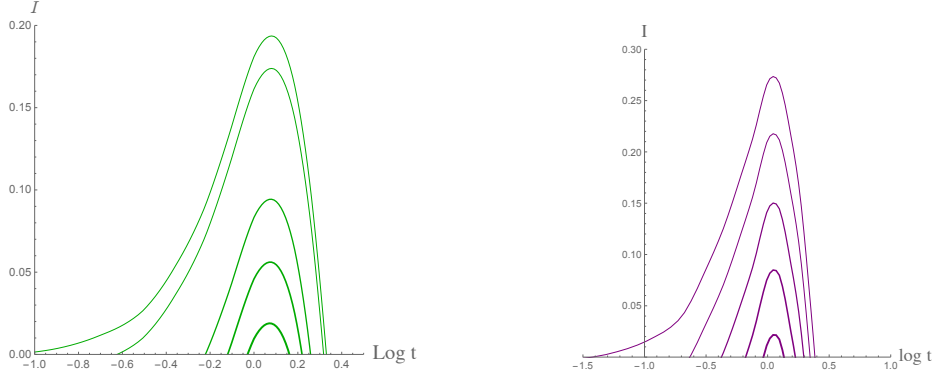


Figure 22. We show typical bell like profiles of the time dependence of the mutual information for Vaidya quenches in the AdS_4 (the left plot) and in the AdS black brane (the right plot).

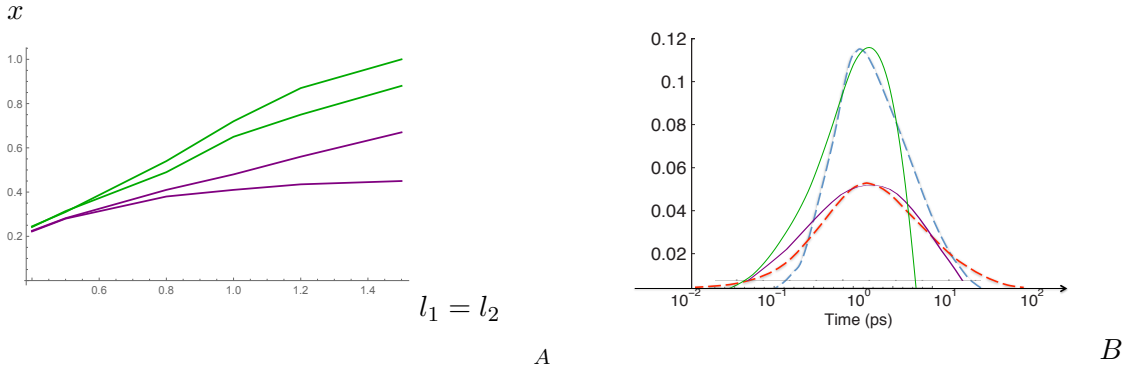


Figure 23. A. The domains corresponding to the bell profiles of time dependence of the mutual information after the Vaidya quench in the AdS_4 (the domain between green lines) and in the AdS black brane (the domain between purple lines) for equal width belts and different distances between them. **B.** The blue and red dashed lines show the time dependence of the mutual information of the reduced FMO system calculated in [50] at 70°K and 300°K temperature, respectively. The green and purple solid lines show the rescaled time dependence of the holographical mutual information for $l_1 = 0.8, l_2 = 0.8$ and $x = 0.5$ and $x = 0.4$ for cases of the global quench in AdS_4 and AdS_4 black brane, respectively.

time t_{scr} at which the mutual information of any two subsystems will be vanishing or small. It was conjectured that black holes are fastest scramblers in nature [64].

Numerical results show that all these time scales depend on the geometry as well as on the form of the quench. Plots in Fig.22 show that the wake up time is very sensitive to the change of distances between segments, while the scrambling time is not so sensitive. In Fig.23.A we show the domains corresponding to the bell profiles of time dependence of the mutual information after the Vaidya quench in the AdS_4 (the domain between green lines) and in the AdS black brane (the domain between purple lines) for equal width belts and different distances between them. We see that the gaps where the bell profiles are available are quite narrow. The gaps corresponding to initial vacuum state and the state

with non-zero temperature are not crossing. By this reason our fitting with results [50] have been performed for different geometries. In the case of infinitely thin shell these time scales admit analytical studies [20].

4 Holographic studies of the FMO complex with one composite part

In this section we consider holographic description of the quantum mutual information for the reduction of the FMO complex with one composite part.

4.1 Phase structure of holographic entanglement entropy $S(A \cup B \cup C)$ for the Vaidya shell in the AdS_d black brane background

In this section we consider the phase structure of holographic entanglement entropy $S(A \cup B \cup C)$ for the Vaidya shell in the three dimensional AdS black brane background with $f = f(z, v)$ given by (2.20) and (2.22), and 3 segments shown in Fig.17, at different times during the quench. This quantity depends on many variables, $l_1, l_2, l_3, x, y, m, m_0$ and α , and we can perform our analysis only numerically, see Fig.24. In these plots contributions of various diagrams to the entanglement entropy for 3 strips, A, B, C , with unequal lengths l_1, l_2, l_3 at different times during the transition from the black brane configuration in AdS_3 with the small mass m_0 to the large mass m are shown. We see that there are plots there the contribution to the holographic entanglement entropy is given by the "engulfed" diagram. These regions are colored yellow in images in Fig.24. The images that contain yellow regions are located at the intersections of the second column and top and middle rows. Hence we have to take into account these diagrams in the analysis of the mutual information. To this purpose we use the diagram technique described in the end of Sect.2.3.

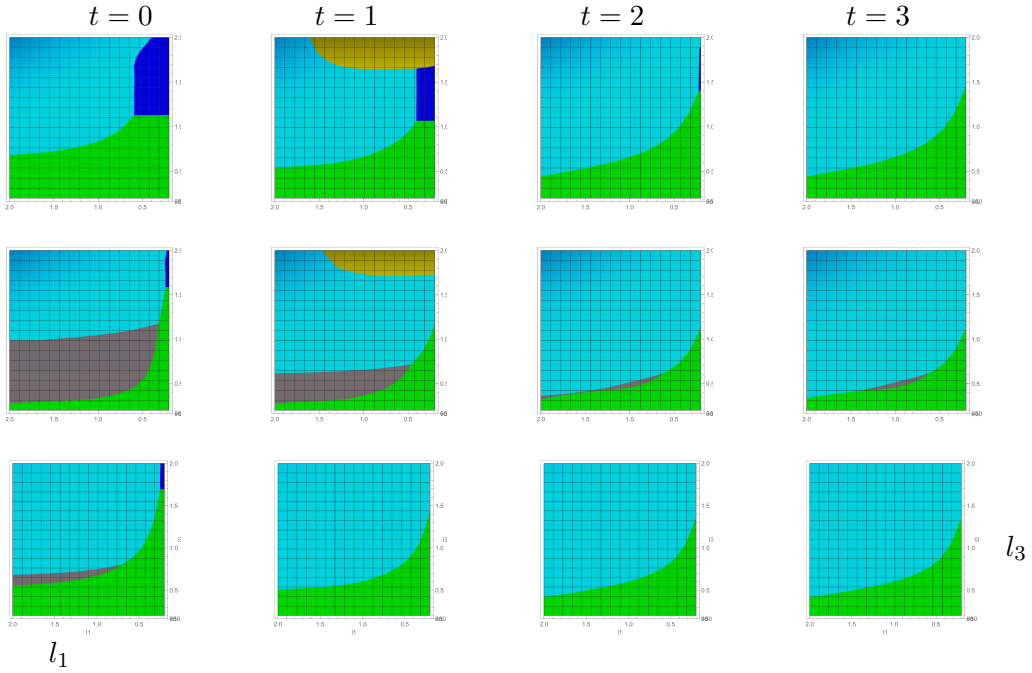


Figure 24. Cartoon diagrams that show the contributions of various diagrams to the entanglement entropy for 3 strips, A, B, C , with unequal lengths l_1, l_2, l_3 at different times during the transition from the black brane configuration with the small mass m_0 to the large mass m in AdS_3 . The green color regions correspond to the bulk surface $(A)||B||C$, the blue color regions correspond to the bulk surface $(A)||BC)_c$, the gray color regions correspond to the bulk surface $(AB)_c||C$, the cyan color corresponds to the bulk surface $(A, B, C)_{c,non-cr}$ and the yellow regions correspond to the bulk surface $(ABc)_c$. Different colors regions are separated by the curves that are the transition lines. In the top plots $l_2 = l_3, x = 0.4, y = 0.4$, in the middle plots $l_2 = l_3, x = 0.2, y = 0.5$ and in the bottom plots $l_2 = 0.5 l_1, x = 0.4, y = 0.5$ and we vary l_1 and l_3 keeping the distances between segments fixed. All plots correspond to $\alpha = 0.2$.

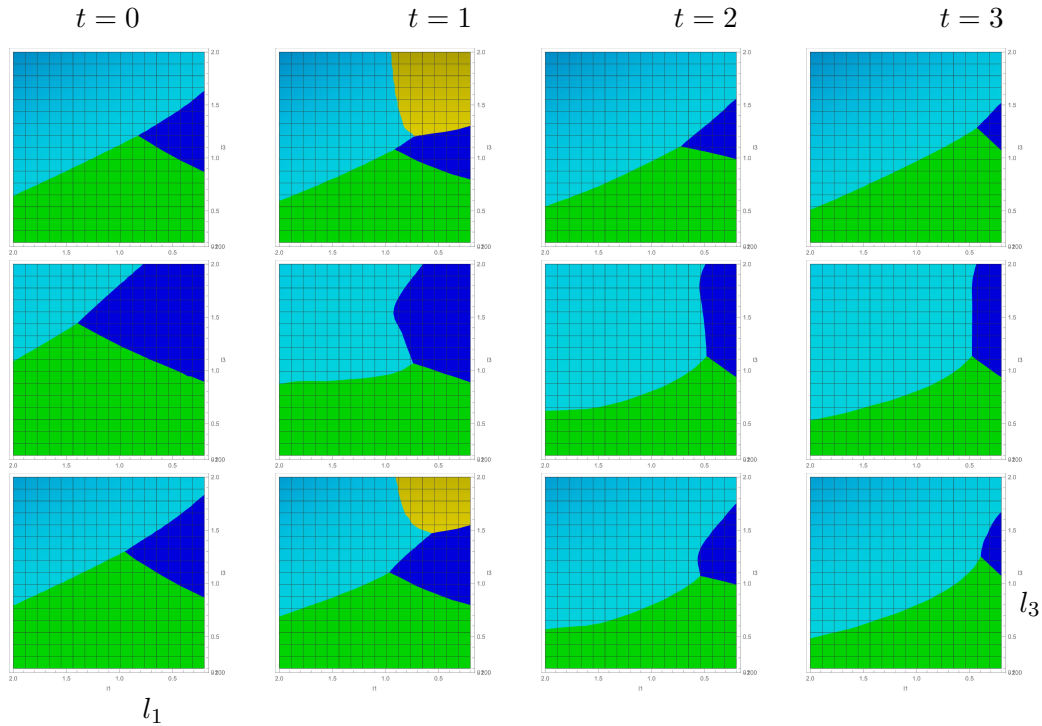


Figure 25. Cartoon diagrams that show the contributions of various diagrams to the entanglement entropy for 3 strips, A, B, C , with unequal lengths l_1, l_2, l_3 at different times during the transition from the black brane configuration with the small mass m_0 to the large mass m in AdS_4 . The green color regions correspond to the bulk surface $(A)||B||C$, the blue color regions correspond to the bulk surface $(A)||BC)_c$, the gray color regions correspond to the bulk surface $(AB)_c||C$, the cyan color corresponds to the bulk surface $(A, B, C)_{c,non-cr}$ and the yellow regions correspond to the bulk surface $(A_B C)_c$. Different colors regions are separated by the curves that are the transition lines. In the top plots $l_2 = l_3, x = 0.5, y = 1$, in the middle plots $l_2 = 0.4l_3, x = 0.4, y = 0.5$ and in the bottom plots $l_2 = 0.5l_1, x = 0.5, y = 1$ and we vary l_1 and l_3 keeping the distances between segments fixed. All plots correspond to $\alpha = 0.2$.

4.2 Mutual information for $(1, 6|3)$ -reduction of the FMO complex and scrambling time

In the section we will consider also the mutual information for a system one part of which consists on two disjoint parts. Just this system corresponds to one of simplest reduce FMO

complexes presented in Fig.2. Applying to this system the general definition (2.38) we get

$$I(A \cup B; C) = S(A \cup B) + S(C) - S(A \cup B \cup C), \quad (4.1)$$

where $S(A \cup B \cup C)$ is the entanglement entropy for the union of three subsystems. $I(A \cup B, C)$ is related with the tripartite information which is defined for a system consisting of three disjoint parts as follows

$$I_3(A; B; C) = S(A) + S(B) + S(C) - S(A \cup B) - S(A \cup C) - S(B \cup C) + S(A \cup B \cup C). \quad (4.2)$$

The tripartite information can be positive, negative or zero, however the holographic tripartite information is always negative, i.e. $I_3(A; B; C) < 0$. The validity of this inequality means that the holographic mutual information is monogamous [15]. The tripartite information can be written in terms of mutual information as follows

$$I_3(A, B, C) = I(A; B) + I(A; C) - I(A; B \cup C). \quad (4.3)$$

We take $A = A_6$, $B = A_1$, $C = A_3$, where A_i , $i = 1, 3, 6$ are 1,3 and 6 sites of the (1,6|3)-reduction of the FMO complex. We assume that A_6, A_3, A_1 are three strips of length l_1, l_2 and l_3 , and separated by distances x and y , Fig.26.

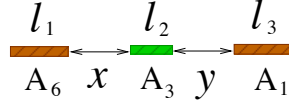


Figure 26. Brown segments show 6 and 1 sites location and the green one shows 3 site location for (1,6|3)-reduction of the FMO complex, depicted in Fig.2.

In the notations introduced in Sect.2.3 and the geometry presented in Fig.26 we can write

$$\mathcal{S}((A_6, A_1)_{joint-ncr}) = \mathcal{S}(l_1 + l_2 + l_3 + x + y, t) + \mathcal{S}(l_2 + x + y, t) \quad (4.4)$$

$$\mathcal{S}((A_6, A_1)_{dis}) = \mathcal{S}(l_1, t) + \mathcal{S}(l_3, t) \quad (4.5)$$

$$\mathcal{S}((A_6, A_1)_{joint-cr}) = \mathcal{S}(l_1 + l_2 + l_3 + x + y, t) + \mathcal{S}(l_2 + l_3 + x + y, t) \quad (4.6)$$

where $\mathcal{S}(l, t)$ is the holographic entropy given by (2.31) or (2.32).

$$S(A_1 \cup A_6) = \min\{\mathcal{S}((A_6, A_1)_{joint-ncr}), \mathcal{S}((A_6, A_1)_{dis}), \mathcal{S}((A_6, A_1)_{joint-cr})\} \quad (4.7)$$

To get $S(A_6 \cup A_3 \cup A_1)$ for three segments we have to take into account the following competing contributions

$$\mathcal{S}((A_6||A_3||A_1)) = \mathcal{S}(l_1, t) + \mathcal{S}(l_2, t) + \mathcal{S}(l_3, t) \quad (4.8)$$

$$\mathcal{S}(A_6||((A_3, A_1)_{ncr})) = \mathcal{S}(l_1) + \mathcal{S}(l_2 + l_3 + y, t) + \mathcal{S}(y, t) \quad (4.9)$$

$$\mathcal{S}((A_6 A_3)_{ncr}||A_1) = \mathcal{S}(l_1 + l_2 + x, t) + \mathcal{S}(x, t) + \mathcal{S}(l_3, t) \quad (4.10)$$

$$\mathcal{S}(A_6 \underbrace{\mathbf{A}_3}_{\text{A}_3} A_1)_{ncr}) = \mathcal{S}(l_1 + l_2 + l_3 + x + y, t) + \mathcal{S}(l_2 + x + y, t) + \mathcal{S}(l_2, t) \quad (4.11)$$

$$\mathcal{S}(A_6 \underbrace{\mathbf{A}_3}_{\text{A}_3} A_1)_{cr}) = \mathcal{S}(l_1 + l_2 + x + y, t) + \mathcal{S}(l_2 + l_3 + x + y, t) + \mathcal{S}(l_2, t) \quad (4.12)$$

$$\mathcal{S}((A_6 A_3 A_1)_{ncr}) = \mathcal{S}(l_1 + l_2 + l_3 + x + y, t) + \mathcal{S}(x, t) + \mathcal{S}(y, t) \quad (4.13)$$

$$\mathcal{S}((A_6 A_3 A_1)_{cr,1}) = \mathcal{S}(l_1 + l_2 + l_3 + x + y, t) + \mathcal{S}(l_2 + x, t) + \mathcal{S}(l_2 + y, t) \quad (4.14)$$

$$\mathcal{S}((A_6 A_3 A_1)_{cr,2}) = \mathcal{S}(l_1 + l_2 + x + y, t) + \mathcal{S}(x, t) + \mathcal{S}(l_3 + y, t) \quad (4.15)$$

$$\mathcal{S}((A_6 A_3 A_1)_{cr,3}) = \mathcal{S}(l_1 + x, t) + \mathcal{S}(l_2 + l_3 + x + y, t) + \mathcal{S}(y, t) \quad (4.16)$$

and

$$\begin{aligned} & S(A_6 \cup A_3 \cup A_1) \quad (4.17) \\ &= \min \left\{ \mathcal{S}((A_6||A_3||A_1)), \mathcal{S}(A_6||((A_3, A_1)_{ncr})), \mathcal{S}((A_6 A_3)_{ncr}||A_1), \mathcal{S}(A_6 \underbrace{\mathbf{A}_3}_{\text{A}_3} A_1)_{ncr}) \right. \\ & \quad \left. \mathcal{S}(A_6 \underbrace{\mathbf{A}_3}_{\text{A}_3} A_1)_{cr}), \mathcal{S}((A_6 A_3 A_1)_{ncr}), \mathcal{S}((A_6 A_3 A_1)_{cr,2}), \mathcal{S}((A_6 A_3 A_1)_{cr,3}) \right\} \end{aligned}$$

Let us note, that for some particular background [23] and refs therein, we can ignore contribution of (4.6), (4.11), (4.14), (4.15) and (4.16).

The time dependence of the holographic mutual information $I(A_6 \cup A_1; A_3)$ for the Vaidya metric in the four dimensional black brane background with $f = f(z, v)$ given by (2.20) and (2.22) ($m_0 = 0.25, m = 1$) and the x_1 -projection of the 3 belts configuration shown in Fig.26, at fixed l_1, l_2, l_3, x, y is presented in Fig.27. The lines of the same style (by the style we mean the color and the type of the line) correspond to the same l_1, l_2, l_3 and y , but different values of x , the distance between the sites "3" and "1" of the FMO complex presented in Fig.2. Fig.28 and Fig. 29 show different plots collected in Fig.27.

We observe that the evolution of the holographic mutual information for the case when one part of the system is consisting from two disjoint subsystems, globally resembles the case of two simple parts, but locally there are some changes. More specifically, as in the case of two simple parts, see Sec.3.2, globally there are 4 different behaviors: the mutual information is 0 at all times; the mutual information starts from a positive value and ends at another positive value; the mutual information starts from a positive value and ends at 0; the mutual information starts from 0, becomes positive for some time and ends at 0 (the bell form of the time dependence). In the context of the FMO complex study, the last case presents a special interest. Locally, we see phase transitions for some particular configurations. These cases are indicated by arrow in Fig.28 and Fig.29.

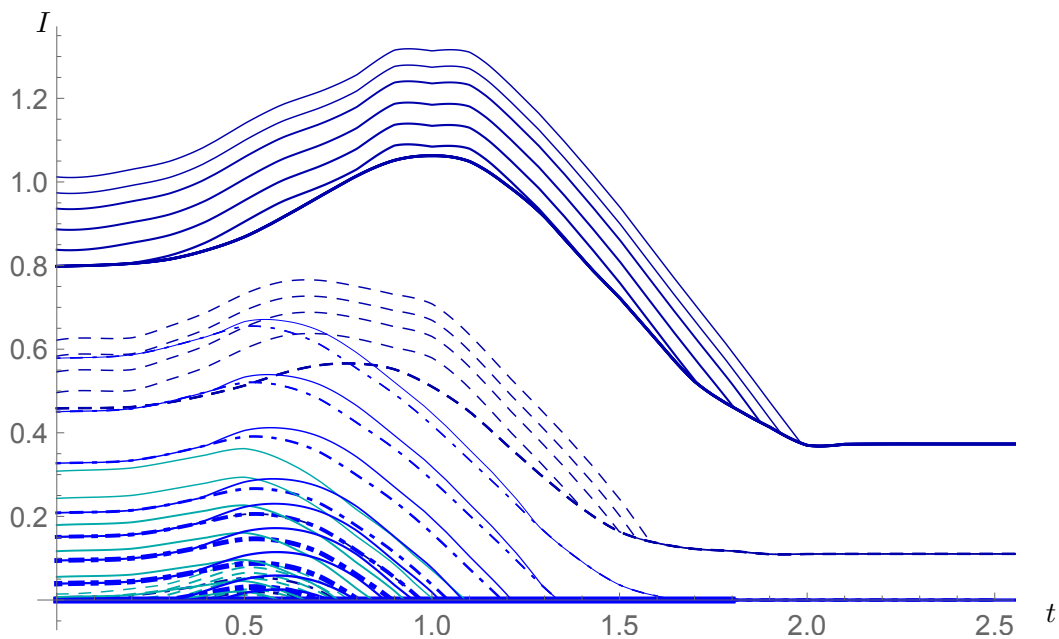


Figure 27. Holographic mutual information $I(A_6 \cup A_1; A_3)$, up to the normalizing factor, for the Vaidya metric in the four dimensional black brane background with $f = f(z, v)$ given by (2.20) and (2.22) ($m_0 = 0.25, m = 1$) and the x_1 -projection of the 3 belts configuration shown in Fig.26, as function of the boundary time t at fixed l_1, l_2, l_3, x, y . The lines of the same style correspond to the same l_1, l_2, l_3 and y , but different values of x , the distance between the sites "3" and "1" of the FMO complex. For more details see Fig.28 and Fig.29.

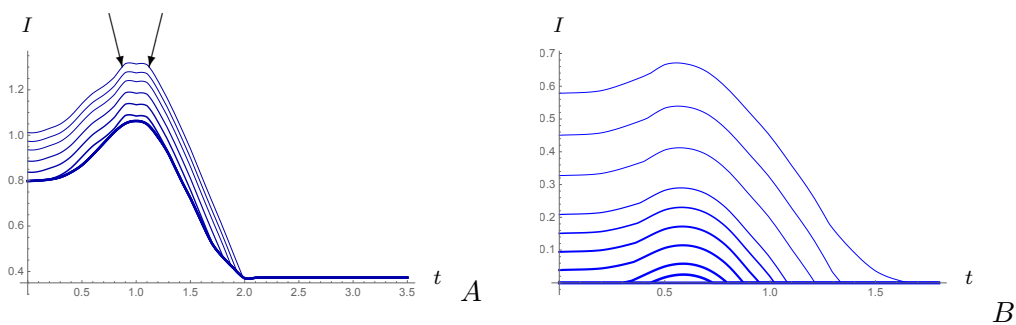


Figure 28. Detailed plots for Fig.27. In plots **A**: $l_1 = 0.3, l_2 = 0.8, l_3 = 0.7, y = 0.3$ and $0.2 < x < 0.24$; in plots **B**: $l_1 = 0.4, l_2 = 0.5, l_3 = 0.4, y = 0.3$ and $0.2 < x < 0.26$. Values of x increase going from the top curve to the bottom one. Arrows indicate the phase transitions.

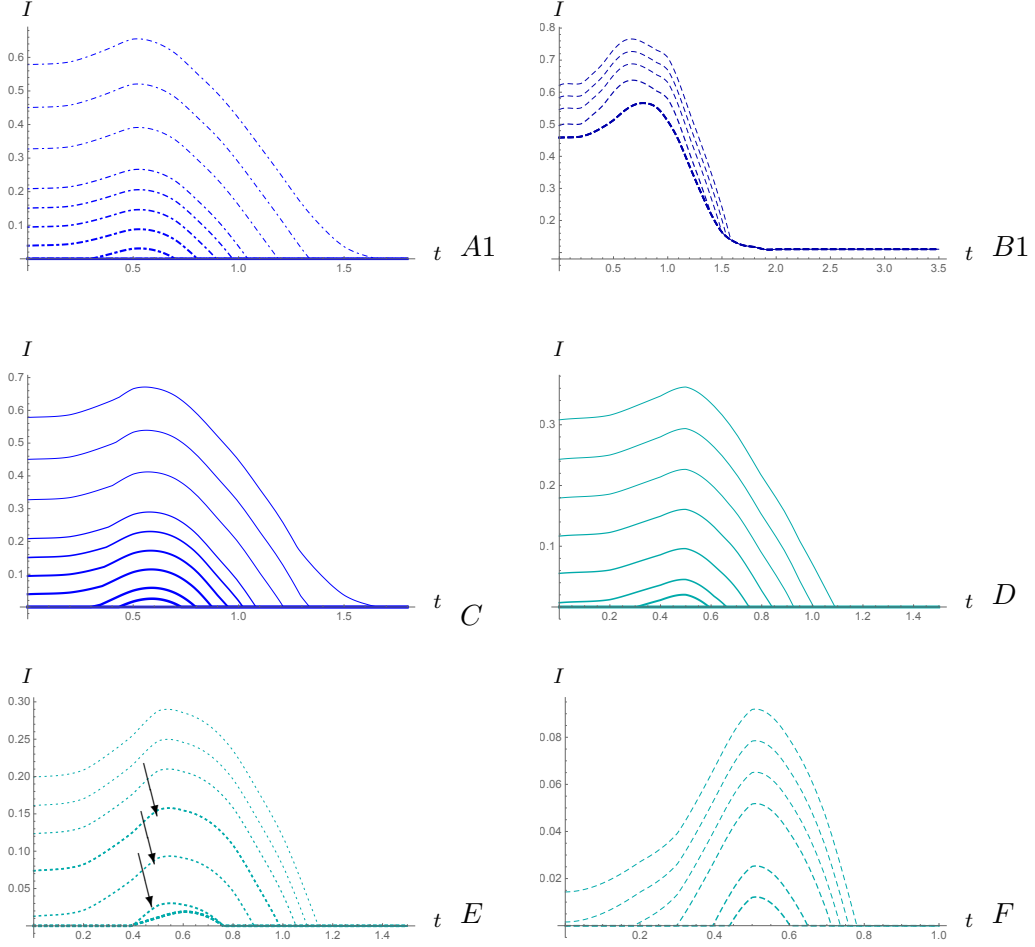


Figure 29. Detailed plots for Fig.27. In plots **A**: $l_1 = 0.4, l_2 = 0.5, l_3 = 0.3, y = 0.3$ and $0.2 < x < 0.26$; **B**: $l_1 = 0.4, l_2 = 0.7, l_3 = 0.3, y = 0.3$ and $0.2 < x < 0.235$. Values of x increase going from the top curve to the bottom one. **C**: $l_1 = 0.4, l_2 = 0.4, l_3 = 0.4, y = 0.3$ and $0.2 < x < 0.26$; **D**: $l_1 = 0.3, l_2 = 0.4, l_3 = 0.5, y = 0.3$ and $0.2 < x < 0.24$; **E**: $l_1 = 0.3, l_2 = 0.4, l_3 = 0.5, y = 0.3$ and $0.2 < x < 0.24$; **F**: $l_1 = 0.3, l_2 = 0.4, l_3 = 0.5, y = 0.3$ and $0.2 < x < 0.206$. Values of x increase going from the top curve to the bottom one. Arrow indicate the phase transitions.

4.3 Matching holographic calculations to the simulation results.

In this subsection we fit some results of numerical simulations for the FMO complex presented in [50] by the holographic description. The mutual information at the physiological temperature ($300^\circ K$) calculated in [50], Fig.3c, when the first system is the site three and the second system is a mixed state of sites one and six is presented in Fig.29 by the red dashed line. The time dependence of the holographic mutual information $I(A_6 \cup A_1; A_3)$

under the global quench by the Vaidya shell in AdS_4 is shown by the dark cyan line also in Fig.29. Note that we make rescaling for this line. We see a rather good fit of these two curves.

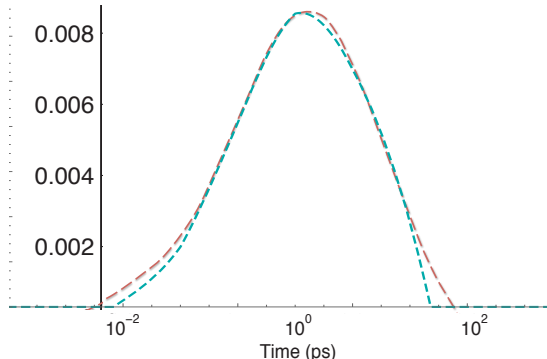


Figure 30. The dashed red curve shows the time dependence (in the logarithmic scale) of the mutual information at the physiological temperature (300°K) calculated in [50], Fig. 3c, when the first system is the site ones and the second system is a mixed state of sites one and six. The time dependence of the holographic mutual information $I(A_6 \cup A_1; A_3)$ under the global quench by the Vaidya shell in AdS_4 is shown by the dark cyan line.

5 Conclusions

We have applied the holographic approach to evaluate the time dependence of entanglement entropy and quantum mutual information in the Fenna-Matthews-Olson protein-pigment complex in green sulfur bacteria during the transfer of an excitation from a chlorosome antenna to a reaction center. It is shown that the time evolution of the mutual information simulating the Lindblad master equation in some cases can be obtained by means of a dual gravity describing black hole formation in the Vaidya AdS spacetime or the Vaidya AdS black brane spacetime. The wake up and scrambling times for various partitions of the FMO complex are discussed. We have demonstrated that some results of numerical simulations [50] for the FMO complex can be fitted by reduced holographic models containing just 2 or 3 segments, Fig.21, Fig.23.B and Fig.30.

To describe another results known for the FMO complex it would be interesting to study more complex holographic models containing 7 or 8 segments. It would be also suitable in this context to change the geometry of disjoint regions and consider, for example, the disk regions. Considering the global AdS_{d+1} one can also study the compact systems. In the case of the global AdS_3 one can consider the time dependence of the mutual information not only during the global quench, described by the Vaidya metric [66], but also during the local quench provided by ultrarelativistic particle in AdS_3 [67]. Studying Lifshitz backgrounds could be useful for describing not only the FMO complex but also other light-harvesting complexes. We suspect that the holographic approach could provide a useful description of certain appropriate quantities not only for quantum photosynthesis but also

for other life science phenomena studied in quantum biology such as the process of vision, the olfactory sense and quantum tunneling in biomolecules.

6 Acknowledgments

I.A. would like to thank Dmitry Ageev for help with numerical calculations. This work was supported by the Russian Science Foundation (grant No. 14-11-00687).

References

- [1] O. Aharony, S. S. Gubser, J. M. Maldacena, H. Ooguri and Y. Oz, “Large N field theories, string theory and gravity,” *Phys. Rept.* **323**, 183 (2000) [hep-th/9905111].
- [2] J. Casalderrey-Solana, H. Liu, D. Mateos, K. Rajagopal, U. A. Wiedemann, “Gauge/String Duality, Hot QCD and Heavy Ion Collisions,” [arXiv:1101.0618 [hep-th]].
- [3] I. Ya. Aref’eva, “Holographic approach to quark-gluon plasma in heavy ion collisions,” *Phys. Usp.* **57**, 527 (2014).
- [4] O. DeWolfe, S. S. Gubser, C. Rosen and D. Teaney, “Heavy ions and string theory,” *Prog. Part. Nucl. Phys.* **75**, 86 (2014) [arXiv:1304.7794 [hep-th]].
- [5] S. A. Hartnoll, C. P. Herzog and G. T. Horowitz, “Holographic Superconductors,” *JHEP* **0812**, 015 (2008) [arXiv:0810.1563 [hep-th]].
- [6] S. Sachdev, “Condensed Matter and AdS/CFT,” *Lect. Notes Phys.* **828**, 273 (2011), [arXiv:1002.2947 [hep-th]].
- [7] S. Ryu and T. Takayanagi, “Holographic derivation of entanglement entropy from AdS/CFT,” *Phys. Rev. Lett.* **96**, 181602 (2006) [hep-th/0603001].
- [8] S. Ryu and T. Takayanagi, “Aspects of Holographic Entanglement Entropy,” *JHEP* **0608**, 045 (2006) [hep-th/0605073].
- [9] V. E. Hubeny, M. Rangamani and T. Takayanagi, “A Covariant holographic entanglement entropy proposal,” *JHEP* **0707**, 062 (2007) [arXiv:0705.0016 [hep-th]].
- [10] V. E. Hubeny and M. Rangamani, “Holographic entanglement entropy for disconnected regions,” *JHEP* **0803**, 006 (2008) [arXiv:0711.4118 [hep-th]].
- [11] M. Headrick, “Entanglement Renyi entropies in holographic theories,” *Phys. Rev. D* **82**, 126010 (2010) [arXiv:1006.0047 [hep-th]].
- [12] J. Abajo-Arrastia, J. Aparicio and E. Lopez, “Holographic Evolution of Entanglement Entropy,” *JHEP* **1011**, 149 (2010) [arXiv:1006.4090 [hep-th]].
- [13] T. Albash and C. V. Johnson, “Evolution of Holographic Entanglement Entropy after Thermal and Electromagnetic Quenches,” *New J. Phys.* **13**, 045017 (2011) [arXiv:1008.3027 [hep-th]].
- [14] V. Balasubramanian *et al.*, “Holographic Thermalization,” *Phys. Rev. D* **84**, 026010 (2011) [arXiv:1103.2683 [hep-th]].
- [15] P. Hayden, M. Headrick and A. Maloney, “Holographic Mutual Information is Monogamous,” *Phys. Rev. D* **87**, no. 4, 046003 (2013) [arXiv:1107.2940 [hep-th]].

- [16] V. Balasubramanian, A. Bernamonti, N. Copland, B. Craps and F. Galli, “Thermalization of mutual and tripartite information in strongly coupled two dimensional conformal field theories,” *Phys. Rev. D* **84**, 105017 (2011) [arXiv:1110.0488 [hep-th]].
- [17] A. Allais and E. Tonni, “Holographic evolution of the mutual information,” *JHEP* **1201**, 102 (2012) [arXiv:1110.1607 [hep-th]].
- [18] R. Callan, J. -Y. He and M. Headrick, “Strong subadditivity and the covariant holographic entanglement entropy formula,” *JHEP* **1206**, 081 (2012) [arXiv:1204.2309 [hep-th]].
- [19] W. Fischler, A. Kundu and S. Kundu, Holographic Mutual Information at Finite Temperature, *Phys. Rev. D* **87**, no. 12, 126012 (2013) [arXiv:1212.4764 [hep-th]].
- [20] H. Liu and S. J. Suh, “Entanglement growth during thermalization in holographic systems,” *Phys. Rev. D* **89**, no. 6, 066012 (2014) [arXiv:1311.1200 [hep-th]].
- [21] Matthew Headrick, ”General properties of holographic entanglement entropy”, *JHEP* 03 (2014) 085, [arXiv:1312.6717 [hep-th]]
- [22] M. Alishahiha, M. R. M. Mozaffar and M. R. Tanhayi, “On the Time Evolution of Holographic n-partite Information,” *JHEP* **1509**, 165 (2015) [arXiv:1406.7677 [hep-th]].
- [23] O. Ben-Ami, D. Carmi and J. Sonnenschein, “Holographic Entanglement Entropy of Multiple Strips,” *JHEP* **1411**, 144 (2014) [arXiv:1409.6305 [hep-th]].
- [24] Curtis T. Asplund, Alice Bernamonti, Federico Galli, Thomas Hartman, ”Entanglement Scrambling in 2d Conformal Field Theory”, *J. High Energy Phys.* 2015:110 (2015), [arXiv:1506.03772 [hep-th]].
- [25] E. Caceres, M. Sanchez and J. Virrueta, “Holographic Entanglement Entropy in Time Dependent Gauss-Bonnet Gravity,” arXiv:1512.05666 [hep-th].
- [26] M. R. Tanhayi, “Thermalization of Mutual Information in Hyperscaling Violating Backgrounds,” arXiv:1512.04104 [hep-th].
- [27] M. R. M. Mozaffar, A. Mollabashi and F. Omid, “Holographic Mutual Information for Singular Surfaces,” *JHEP* **1512**, 082 (2015) [arXiv:1511.00244 [hep-th]].
- [28] I. Ya. Aref’eva, A. A. Golubtsova and E. Gourgoulhon, “Analytic black branes in Lifshitz-like backgrounds and thermalization,” arXiv:1601.06046 [hep-th].
- [29] S. Kundu and J. F. Pedraza, “Spread of entanglement for small subsystems in holographic CFTs,” arXiv:1602.05934 [hep-th].
- [30] N. Sircar, J. Sonnenschein, W. Tangarife, ”Extending the scope of holographic mutual information and chaotic behavior” , [arXiv:1602.07307 [hep-th]].
- [31] S. Mirabi, M. R. Tanhayi and R. Vazirian, “On the Monogamy of Holographic n -partite Information,” arXiv:1603.00184 [hep-th].
- [32] Markus Arndt, Thomas Juffmann, and Vlatko Vedral, ”Quantum physics meets biology,” *HFSP J.* 2009 Dec; 3(6): 386400.
- [33] Graham R. Fleming, Gregory D. Scholes, Yuan-Chung Cheng, ”Quantum effects in biology,” *Procedia Chemistry* 3 (2011) 3857.
- [34] Masanori Ohya, Igor Volovich, *Mathematical Foundations of Quantum Information and Computation and Its Applications to Nano- and Bio-systems*, Springer, 2011.

- [35] *Quantum Bio-Informatics IV*, eds. L. Accardi, W. Freudenberg, and M. Ohya, World scientific, 2011.
- [36] *Quantum Effects in Biology*, eds. Masoud Mohseni, Yasser Omar, Gregory S. Engel, Martin B. Plenio, Cambridge University Press, 2014.
- [37] Igor V. Volovich, "Cauchy-Schwarz inequality-based criteria for the non-classicality of sub-Poisson and antibunched light", *Phys. Lett. A*, 380:1-2 (2016), 56-58.
- [38] R.E. Blankenship, *Molecular Mechanism of Photosynthesis*, (Blackwell Science, London, 2002).
- [39] R. E. Fenna and B. W. Matthews. "Chlorophyll arrangement in a bacteriochlorophyll protein from chlorobium limicola", *Nature*, 258, 573-577, December 1975.
- [40] G.S. Engel, T.R. Calhoun, E.L. Read, T.-K. Ahn, T. Man'cal, Y.-C. Cheng, R.E. Blankenship, G.R. Fleming, "Evidence for wavelike energy transfer through quantum coherence in photosynthetic systems", *Nature*, 446 (2007) 782.
- [41] Collini, E.; Wong, C. Y.; Wilk, K. E.; Curmi, P. M. G.; Brumer, P.; Scholes, G. D. "Coherently Wired LightHarvesting in Photosynthetic Marine Algae at Ambient Temperature", *Nature*, 2010, 463, 644.
- [42] G. Panitchayangkoon, D. Hayes, K.A. Fransted, J.R. Caram, E. Harel, J. Wen, R.E. Blankenship, G.S. Engel, "Long-Lived Quantum Coherence in Photosynthetic Complexes at Physiological Temperature," *Proc. Natl. Acad. Sci. USA* 107 (2010) 12766-12770.
- [43] G.D. Scholes, G.R. Fleming, A. Olaya-Castro, R. van Grondelle, "Lessons from nature about solar light harvesting", *Nature Chem.*, 2011, 3, 763774.
- [44] T.R. Calhoun, N.S. Ginsberg, G.S. Schlau-Cohen, Y.-C. Cheng, M. Ballottari, R. Bassi, G.R. Fleming, "Quantum Coherence Enabled Determination of the Energy Landscape in Light-Harvesting Complex II", *J. Phys. Chem. B* 113 (2009) 16291.
- [45] E. Collini, C.Y. Wong, K.E. Wilk, P.M.G. Curmi, P. Brumer, G.D. Scholes, Coherently wired light-harvesting in photosynthetic marine algae at ambient temperature, *Nature* 463 (2010) 644.
- [46] H. Lee, Y.-C. Cheng, G.R. Fleming, "Coherence dynamics in photosynthesis: protein protection of excitonic coherence", *Science* 316 (2007) 1462.
- [47] Masoud Mohseni, Patrick Rebentrost, Seth Lloyd, and Alan Aspuru-Guzik. Environment-assisted quantum walks in photosynthetic energy transfer. *The Journal of Chemical Physics*, 129(17):174106, 2008.
- [48] F. Caruso, A.W. Chin, A. Datta, S.F. Huelga, M.B. Plenio, "Highly efficient energy excitation transfer in light-harvesting complexes: The fundamental role of noise-assisted transport", *J. Chem. Phys.* 131 (2009) 105106.
- [49] M. Sarovar, A. Ishizaki, G.R. Fleming, K.B. Whaley, "Quantum entanglement in photosynthetic light harvesting complexes", *Nature Physics*, 6:462-467, April 2010.
- [50] Kamil Bradler, Mark M. Wilde, Sai Vinjanampathy, Dmitry B. Uskov, "Identifying the quantum correlations in light-harvesting complexes", *Phys. Rev.A* 82, 062310 (2010), [arXiv:0912.5112 [quant-ph]].
- [51] F. Caruso, A.W. Chin, A. Datta, S.F. Huelga, M.B. Plenio, "Entanglement and entangling power of the dynamics in light-harvesting complexes", *Phys. Rev. A* 81 (2010) 062346.

- [52] Ming-Jie Tao, Qing Ai, Fu-Guo Deng, Yuan-Chung Cheng, "Energy transfer pathway probed by single-molecule pump-dump experiment," [arXiv:1511.01461 [physics.chem-ph]].
- [53] Charlotta Bengtson, Michael Stenrup, and Erik Sjoqvist, "Quantum nonlocality in the excitation energy transfer in the Fenna-Matthews-Olson complex," arXiv:1502.07842 [quant-ph].
- [54] M. Schmidt am Busch, F. Muh, M. E.-A. Madjet, and T. Renger, "The eighth bacteriochlorophyll completes the excitation energy funnel in the FMO protein", J. Phys. Chem. Lett. **2**(2), 93-98 (2011).
- [55] L. Accardi, Yu.G. Lu, and I. Volovich, *Quantum theory and its stochastic limit*, Springer, 2002.
- [56] I. Ya. Aref'eva, I. V. Volovich, S. V. Kozyrev, "Stochastic limit method and interference in quantum many-particle systems", Theoretical and Mathematical Physics, 2015, 183:3, 782–799.
- [57] S.V. Kozyrev and I.V. Volovich, "Dark states in quantum photosynthesis," arXiv:1603.07182.
- [58] A. S. Trushechkin, I. V. Volovich, "Perturbative treatment of inter-site couplings in the local description of open quantum networks", EPL, 113:3 (2016), 30005.
- [59] I. Ya. Aref'eva and I. V. Volovich, On holographic thermalization and dethermalization of quark-gluon plasma; Theor. Math. Phys. **174**, 186 (2013) [Teor. Mat. Fiz. **174**, 216 (2013)], arXiv:1211.6041 [hep-th].
- [60] M. Alishahiha, A. F. Astaneh and M. R. M. Mozaffar, "Thermalization in Backgrounds with Hyperscaling Violating Factor," arXiv:1401.2807 [hep-th].
- [61] P. Fonda, L. Franti, V. Keranen, E. Keski-Vakkuri, L. Thorlacius and E. Tonni, "Holographic thermalization with Lifshitz scaling and hyperscaling violation," arXiv:1401.6088 [hep-th].
- [62] I. Y. Aref'eva, "Formation time of quark-gluon plasma in heavy-ion collisions in the holographic shock wave model," Teor. Mat. Fiz. **184**, no. 3, 398 (2015) [Theor. Math. Phys. **184**, no. 3, 1239 (2015)]. arXiv:1503.02185 [hep-th].
- [63] I. Y. Aref'eva and I. V. Volovich, "The master field for QCD and q deformed quantum field theory," Nucl. Phys. B **462**, 600 (1996), [hep-th/9510210].
- [64] Y. Sekino and L. Susskind, "Fast Scramblers," JHEP **0810**, 065 (2008) [arXiv:0808.2096 [hep-th]].
- [65] P. Caputa, J. Simn, A. Stikonas, T. Takayanagi and K. Watanabe, "Scrambling time from local perturbations of the eternal BTZ black hole," JHEP **1508**, 011 (2015) [arXiv:1503.08161 [hep-th]].
- [66] V. Ziogas, "Holographic mutual information in global Vaidya-BTZ spacetime," JHEP **1509**, 114 (2015) [arXiv:1507.00306 [hep-th]].
- [67] D. S. Ageev and I. Y. Aref'eva, "Holographic Dual to Conical Defects: II. Colliding Ultrarelativistic Particles," arXiv:1512.03363 [hep-th].